No 727481 RESERVE

D3.2 v1.0

Extension to new approaches to high RES contexts

The research leading to these results has received funding from the European Union's Horizon 2020 Research and Innovation Programme, under Grant Agreement no 727481.

Project Name	RESERVE
Contractual Delivery Date:	30.09.2017
Actual Delivery Date:	30.09.2017
Contributors:	Conor Murphy (UCD), Andrew Keane (UCD). Sriram Karthik Gurumurthy (RWTH), David Ryan (WIT), Miguel Ponce De Leon (WIT)
Workpackage:	WP3 – Voltage Control
Security:	PU
Nature:	R
Version:	1.0
Total number of pages:	59

Abstract
This document summarises the voltage control and dynamic voltage stability research concepts completed as part of the RESERVE project. Two concepts have been developed within WP3 that make best use of inverter-based RES units. The concepts operate on differing time scales and fulfil differing objectives. To enable further demonstration on physical hardware and the deployment of the techniques in a field-trial environment both voltage control scenarios warrant extensive experimentation for verification, development and as proof-of-concept. This deliverable (3.2) presents these experiments and reveals the step-by-step guide to developing and applying the voltage control scenarios to distribution networks.

Keyword list
Voltage Control, Voltage Management, Voltage Stability, Active Distribution Systems, 100% RES Energy Networks, Optimisation, Reactive Power.

Executive Summary

This deliverable presents developed methodologies of two voltage control scenarios. These methodologies have been developed within **Task 3.2**, so named as SV_A and SV_B respectively in **WP 1**. RWTH have developed an expansion of **the Middlebrook theory** to an AC and unbalanced context, while UCD put forward an **Active Voltage Management (AVM)** technique. Prior to field-trial deployment and demonstration on physical hardware, both voltage control scenarios warrant extensive experimentation for verification, development and as proof-of-concept. This deliverable (3.2) presents these experiments and reveals the step-by-step guide to developing and applying the voltage control scenarios to distribution networks.

In Chapter 2 a voltage stability analysis of grid-connected inverter is undertaken and extended for the case of an active grid. The stability analysis of grid-connected inverters is performed and corresponding time domain simulations are carried out. The results presented in this chapter validate the coherence between *theoretical modelling* and *time domain simulations*. The influence and impact of Phase Locked Loop (PLL) for power inverters is described and the required changes in the mathematical modelling of inverters is examined. Further verification is achieved in an exemplary 3-node LV feeder presenting a case-study of an active gird where the voltage stability analysis developed in Task 3.2 is applied. Two test cases are formulated on the basis of grid connection. The grid connected LV feeder represents the tightly regulated case and the islanded grid case forms the loosely coupled Microgrid case. The simulation results achieved in Chapter 2 validate the **Dynamic Voltage Stability Monitoring** technique.

In Chapter 3 a voltage management technique is put forward, capitalising on the reactive power capabilities of inverter-based RES units to achieve a desired objective of a distribution system operator on a continual basis. A four-stage offline analysis is presented that provides the means to determine a dynamic relationship between the voltage at the terminals of a RES and its reactive power operation. This relationship, known as a *volt-var curve* makes possible the decentral operation of RES for voltage management. The offline modelling environment is presented in this chapter. A case study using a real LV feeder with 74 customers is examined, in a simulation environment, to investigate two preliminary objectives. Two volt-var curves are formulated for each RES unit in the case-study to achieve the **minimisation of voltage unbalance** and, separately, the **minimisation of active power losses**. The simulation results achieved in Chapter 3 validate the **Active Voltage Management** technique.

In Chapter 4 monitoring concepts and requirements on the scalability of voltage control and stability techniques are addressed. Looking toward future Tasks within **WP3**, the ICT requirements become more pertinent to facilitate an increase in the Technology Readiness Level (TRL) of both voltage techniques. Preliminary investigations of how both voltage control strategies may be deployed are complete. This chapter documents initial findings of the implementation, deployment and puts forward a policy based strategy for *grid code violation* and *collision control*. Initial implementation of software based network codes is also presented.

Deliverable 3.2 presents the successful implementation and validation of the voltage control techniques on representative test networks in a simulation environment. This research effort facilitates the trialling of the techniques in a real distribution system environment in **WP4** and **WP5**, further advancing the TRL to technology development and demonstration stages.

Authors

Partner	Name	e-mail
UCD		
	Conor Murphy	cmurphy5@ucd.ie
	Andrew Keane	andrew.keane@ucd.ie
RWTH		
	Sriram Karthik Gurumurthy	sriram.karthik.gurumurthy@rwth-aachen.de
WIT		
	David Ryan	dryan@tssg.org
	Miguel Ponce De Leon	miguelpdl@tssg.org

Table of Contents

Executive Summary 2
1. Introduction 6
1.1 Task 3.2 6
1.2 Objectives of the Work Report in this Deliverable 6
1.3 Outline of the Deliverable 6
1.4 How to Read this Document 6
1.5 Approach used to Undertake the Work 7
2. Voltage stability analysis of grid connected inverter and extensions for the case of an active grid 8
2.1 Description of grid connected inverter 8
2.1.1 Formulation of stability criteria 8
2.2 Simulation test cases 10
2.2.1 Test scenario description 10
2.2.2 Stable scenarios 11
2.2.2.1 Case 1: Lightly damped case 11
2.2.2.2 Case 2: Highly damped case 12
2.2.3 Results 12
2.3 Impact of phase locked loop (PLL) 12
2.3.1 PLL Modelling 13
2.3.2 Modelling of grid connected inverters with PLL 13
2.4 Extensions to an active grid 14
2.4.1 3 Node LV feeder description 14
2.4.2 Grid Connected Mode 14
2.4.3 Islanded grid Mode 15
2.5 Stability analysis 15
2.5.1 Case 1: Grid connected mode 15
2.5.1.1 Stable operation of Inverter 1 15
2.5.1.2 Unstable operation of Inverter 1 16
2.5.1.3 Result 17
2.5.2 Case 2: Islanded mode 17
2.5.2.1 Stable case 17
2.5.2.2 Unstable case 18
2.5.2.3 Result 18
2.6 Conclusion and future work 18
3. Voltage management using inverter-based RES units 20
3.1 The Active Voltage Management Technique 20
3.2 Multi-Scenario ZIP Diversification 20
3.2.1 Generation Profiles 22
3.3 3-OPF modelling tool 23
3.3.1 Determination of the volt-var curves 24
3.3.1.1 Stage I – Optimal voltage setting 24
3.3.1.2 Stage II – Minimal voltage deviation 25
3.3.1.3 Stage III – Representative voltage calculation 26
3.3.1.4 Stage IV – Formulation of volt-var curves using linear regression 26
3.3.2 Summary 27
3.4 Case Study 27
3.4.1 Network 28
3.4.2 Offline Modelling - Calculation of Volt-var curves 29

3.4.2.1 Minimisation of Voltage Unbalance 29
3.4.2.2 Active Power Loss Minimisation 30
3.4.2.3 Summary of findings 32
3.4.3 Online Deployment - Verification of Volt-var curves 32
3.4.3.1 Results 34
3.5 Conclusions and future work 35
4. ICT Monitoring Concepts 37
4.1 Communication Requirements for Simulations 37
4.1.1 Data Access for Simulations 37
4.1.2 Data Gathering for Simulations 37
4.2 Implementation 38
4.3 Deployment of the Research Concepts 38
4.4 Policy Based Management 39
4.4.1 Scenario 1: Voltage Control research concept output causing violation of the Network Codes 40
4.4.2 Scenario 2: Data Concurrency and Message Collision 41
4.5 Software Implementation of Network Codes 42
5. Conclusion 43
6. References 44
7. List of Abbreviations 46
8. List of Figures 48
9. List of Tables 49
Annex 50
A.1 Additional elements of the DVSM 50
A.1.1 Grid Connected Case System parameters 50
A.1.2 Grid impedance modelling 51
A.1.3 Inverter impedance modelling 51
A.1.4 3-node LV feeder parameter 52
A.2 Additional elements of the AVM technique 54
A.3 Codified Network Codes 56

1. Introduction

This deliverable is the output of Task 3.2 in WP3. This task extends the work of T3.1 to include the formulation of the techniques developed for voltage stability and control in an active grid case. Two complementary techniques for voltage control are being developed in RESERVE that seek to maintain steady-state operation of voltages on power systems with 100% RES. In **WP 1** voltage control scenarios, named SV_A and SV_B, are introduced. This deliverable (3.2) contains the scientific content and presents the assumptions upon which the techniques are built.

The overall objective of Task 3.2 is to provide validation of the developed voltage control techniques by way of simulations on test-case distribution systems. To this end a step-by-step guide is presented for both SV_A and SV_B, herein referred to as the **Dynamic Voltage Stability Monitoring (DVSM)** technique and the **Active Voltage Management (AVM)** technique, respectfully.

1.1 Task 3.2

This deliverable summarises the activities of **Task 3.2** within the wider context of WP3. The aim of WP3 is to bring about a new understanding for the changing landscape that 100% RES uptake will have on distribution networks. **WP3** explores new concepts and theories surrounding steady state voltage regulation and dynamic voltage stability. Two methodologies have been developed within Task 3.1 and Task 3.2, the expansion of **the Middlebrook theory** to an AC and unbalanced context and, separately, the **AVM** technique.

These techniques offer different services to distribution systems hosting inverter-based RES units. The **DVSM** technique is a methodology to *enhance voltage stability* through the identification and modification of system impedances. The **AVM** technique is a methodology to *manage steady state voltages* in the presence of RES while accomplishing an objective at the discretion of the DSO. As both concepts function over differing time-scales they are capable of operating in parallel.

1.2 Objectives of the Work Report in this Deliverable

- To provide the scientific background and assumptions behind the voltage control and stability techniques,
- To provide a valid simulation test-bed for developing and investigating the techniques,
- To produce valid simulations of the voltage control and stability techniques,
- To investigate system level monitoring concepts for ICT for the voltage control and stability techniques,
- To provide an outline of future deliverables and further work.

1.3 Outline of the Deliverable

The deliverable details the research efforts completed in the first year of the RESERVE project in developing the voltage control and stability concepts. The accomplishments within the task exceed that written in the description of work, as steady-state regulation of voltages is also addressed in the AVM technique. The scientific background, simulation platforms, and validation on sample distribution networks are presented here. In developing these concepts in a lab environment, simulation studies are undertaken and, in coordination with ICT partners, monitoring conceptions and requirements on the scalability of these techniques are addressed.

1.4 How to Read this Document

The present deliverable covers the realisation of the voltage control and stability techniques. This document can be read in isolation to other deliverables, yet it follows an introductory deliverable (**D3.1**) that reports on the basic requirements of the voltage control and stability concepts.

Figure 1.1 shows the placement of this deliverable (**D3.2**) in the wider context of **WP3** as well as interlinked work packages of the RESERVE project:

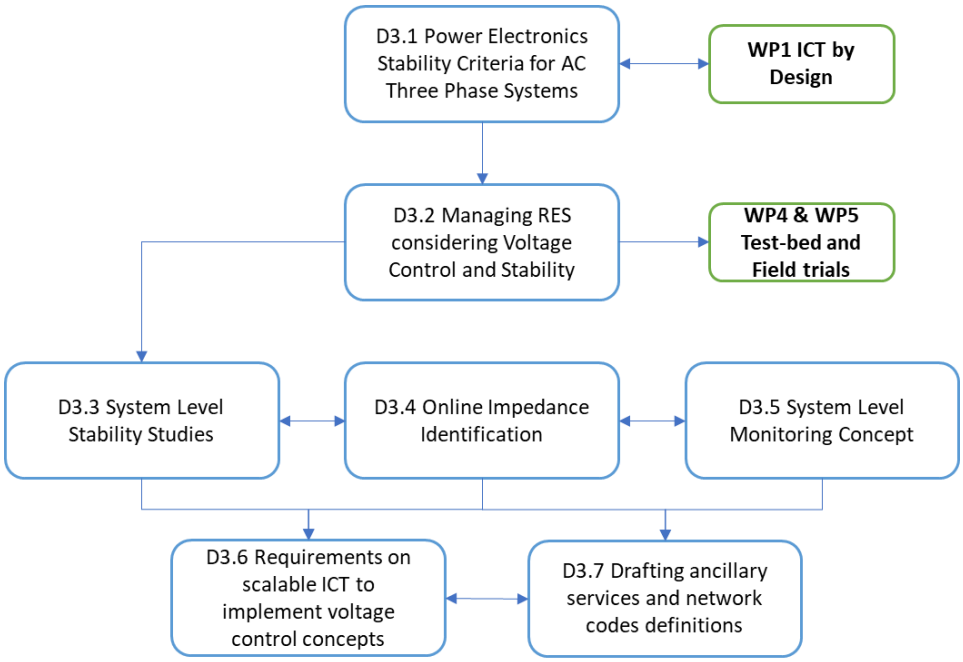

Figure 1.1 Relations between Deliverables in WP3 and other work packages

1.5 Approach used to Undertake the Work

The following steps were applied to develop the results reported in this deliverable.

- The foundation of the new approaches to voltage stability and control are expanded upon from **D3.1** to a simulation environment in **D3.2**.
- Mathematical modelling governs the performance of the Dynamic Voltage Stability Monitoring technique and the AVM technique. The formulation of both techniques is put forward in this deliverable, expanding the application of inverter-based RES units to a case-study context.
- Step-by-step methodologies are developed to outline the replicability of the approach to any distribution feeder context irrespective of the differing inverter-based RES technology.
- Case studies are performed to validate the techniques in using time-domain simulations and time-series power flow.
- Conclusions are drawn based upon the performance of the voltage control techniques in the simulation environment.
- Based on the results of the case studies, a look toward future deliverables and associated work packages is provided.

2. Voltage stability analysis of grid connected inverter and extensions for the case of an active grid

The goal of this chapter is to perform voltage stability analysis for grid connected inverters and provide extensions for the case of an active grid. An exemplary 3 node LV feeder is considered to represent the case of an active grid. The previous deliverable D3.1 researched on existing methods based on Middlebrook theory [1]–[3], which are mainly for DC systems. Extensions of the theory suitable for AC systems was identified as the Generalized Nyquist Criterion (GNC) [4]–[6] in D3.1. The GNC method is adopted for this deliverable and applied to the grid connected inverter test case and to the extended case of an active grid.

The organization of this chapter is as follows. First, a description of a single grid connected inverter is considered and its corresponding stability analysis and simulation results are presented. Furthermore, the impacts of PLL for the inverter system is investigated. The last part of the chapter performs an extended analysis for the 3 node LV feeder. Here two possibilities pertaining to having grid connection is considered. In one of the test case, the 3 Node LV feeder has grid connection. Hence all the three inverters involved are assumed to be operated in current controlled mode. These inverters regulate their output current to the desired reference. In the other test case, one of the inverter is operated in voltage controlled mode and the other two inverters operate in current controlled mode, thus forming a Microgrid.

2.1 Description of grid connected inverter

Consider a three-phase grid connected inverter suited for PV applications. For simplicity, consider the case where the inverter is operated in current mode. The inverter is made to act as a current source through a current controller. The DC side dynamics of the inverter are also neglected to make a clearer case study without involving too many variables or factors. A constant DC voltage source represents the DC side. The three-phase inverter consists of electrical switches connected in a B6C configuration. The switches would be based on either IGBT or MOSFET technology depending on the current rating of the inverter. At the output of the inverter, an LC low pass filter is present which filers out of the higher order harmonics in the current waveform.

2.1.1 Formulation of stability criteria

The basic schematic of the inverter with its current control is presented in Figure 2.1. The diagram is divided into three parts for lucid understanding. In the power stage, the PV panels, the inverter and the LC filter which connects to the grid are shown. The inductor (L_t) also contains an internal coil resistance (R_t) and the equivalent impedance is represented by the solid black block in Figure 2.1. The measurements obtained are the grid voltage and the inductor current denoted by v_{abc} and i_{abc} respectively. The measurement and pre-processing (such as abc to dq frame conversion) for generating the reference angle θ, a PLL is used, which utilises the v_{abc} measurements. The measured inductor current i_{abc} is converted into dq to get i_d and i_q which is used by the current controller for synthesising control commands.

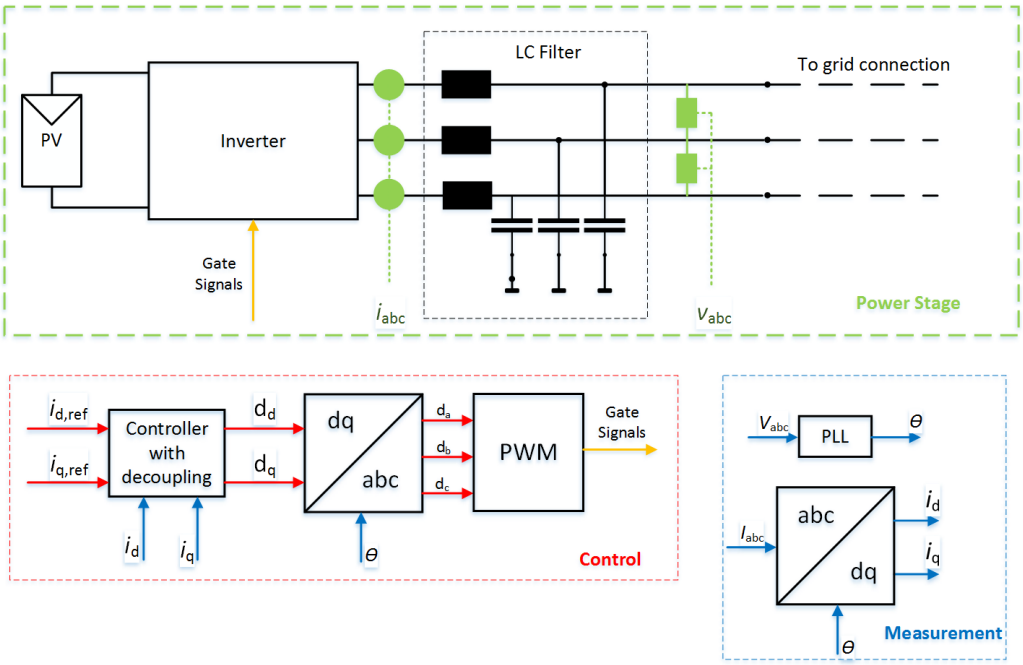

Figure 2.1 Inverter with current control structure

The current controller receives an internal current reference i_{d_ref} and i_{q_ref} from the power controller. In this scenario, the reference for the current control is fixed manually. The current controller synthesises control commands d_d and d_q based on the error between the actual reference command and the measured current values. A proportional-integral (PI) based controller is used for this purpose. The gains of the controller are chosen to achieve suitable bandwidth and phase margin such that the system has sufficient robustness margins. The controller also has a decoupling unit, which decouples the dynamic interaction between i_d and i_q. The block diagram of the current controller can be found in Figure 2.2. The control commands d_d and d_q are converted back to abc frame using the inverse transformation block to get d_a, d_b and d_c as shown in Figure 2.1. The pulse width modulation (PWM) block compares the control commands d_a, d_b and d_c with a triangle wave whose frequency equals the switching frequency of the inverter; to synthesize 'ON' or 'OFF' commands for the switches in the inverter bridge. This method of PWM generation is known as Sine-Triangle PWM [7]. Another sophisticated yet elegant and widely solution for PWM generation is the Space Vector Modulation (SVM) [8]. For SVM implementations, d_d and d_q obtained from the controller are converted to d_α and d_β, which are the inputs for the SVM PWM algorithm. The switching commands from the PWM unit is denoted as gate signals in Figure 2.1and these signals are inputs to the inverter bridge in the power stage.

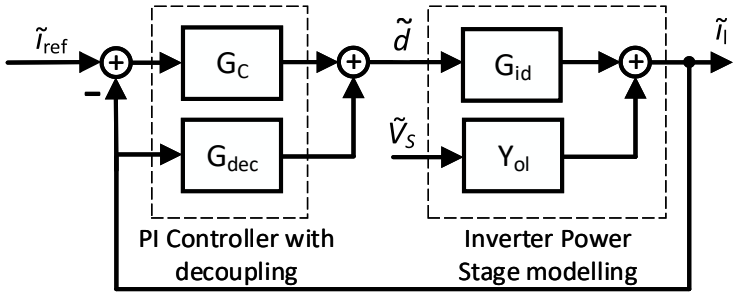

Figure 2.2 Closed loop model of three-phase grid-connected inverter

The inverter power stage modelling is done based on [9] which considers the case of an L filter in the power stage, however in the considered scenario, an LC filter is used. Modifications related to mathematical modelling with regards to an LC filter are accounted for and the corresponding equations can be found in annex A.1. Modelling of the inverter is done in dq frame and the closed loop control diagram of the inverter is shown in Figure 2.2. Due to coupling between d and q axis, the resultant system is a multiple-input-multiple-output (MIMO) system. Notations such as $\tilde{d}$, $\tilde{i}_l$ and $\tilde{i}_{ref}$ represent a vector consisting of both d and q components. Therefore, all the transfer functions such as G_{id}, Y_{ol} etc in Figure 2.2 are 2x2 matrices (containing 4 components) as shown in equation (2.1).

$$G_{id} = \begin{bmatrix} G_{id,dd} & G_{id,dq} \\ G_{id,qd} & G_{id,qq} \end{bmatrix} \tag{2.1}$$

The open loop output admittance of the inverter without considering the feedback path is Y_{ol}. Note that the admittance is the inverse of impedance. The closed loop output admittance Y_{cl} of the inverter is computed considering the feedback path. The mathematical expressions are shown in the annex.

To comprehend system stability, the transfer function of the grid impedance is required for applying the stability test through GNC. Until deliverable D3.3, the components present in the grid are assumed to be known and hence the grid impedance from any given point of common coupling (PCC) can be formulated mathematically and can be computed for a given operating point. This will enable system stability verification from a theoretical frequency domain perspective and a simulation based time domain perspective. From D3.4 onwards, the grid impedances are identified in real time using wideband system identification (WSI) techniques [10]–[14].

2.2 Simulation test cases

In this section, the simulation scenarios are explained and the corresponding simulation results are portrayed and analysed.

2.2.1 Test scenario description

The voltage source converter (VSC) or in other words the grid tied inverter is operated in current mode. The basic setup is illustrated in Figure 2.3. A VSC feeds into the grid in the presence of a local resistive load. The point of interconnection with the local grid terminal is marked as PCC. The grid impedance as seen from the local PCC is denoted by Z_G and the input impedance of the inverter is Z_{inv}. The initial grid impedance is Z_{g1}. Two scenarios are defined based on two different grid impedances Z_{g2} and Z_{g3}. These impedances are connected one at time with the appropriate switch positions. The impact of step change in reference command (i_{d_ref} and i_{q_ref}) for the current controller is studied and the response in time domain is recorded. The initial reference command is 200A and 0A for d and q axis respectively.

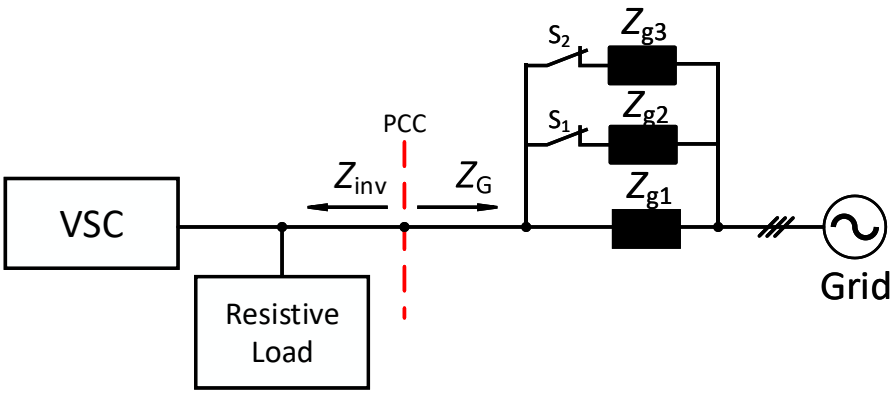

Figure 2.3 Simulation scenarios

2.2.2 Stable scenarios

Case 1 is defined with S1 closed and S2 open and case 2 is defined by S1 open and S2 closed. Depiction of an unstable scenario is not possible with this simple simulation setup. The annex contains the inverter parameters, grid impedance parameters and the control parameters.

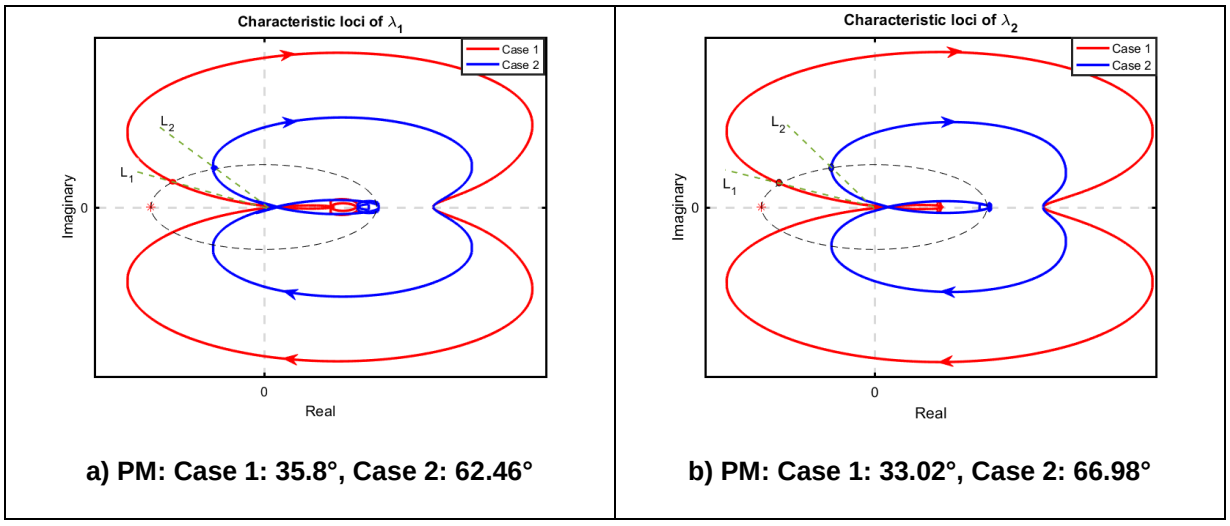

a) PM: Case 1: 35.8°, Case 2: 62.46°

b) PM: Case 1: 33.02°, Case 2: 66.98°

Figure 2.4 Stability analysis results

2.2.2.1 Case 1: Lightly damped case

In this the case, the grid impedance is the parallel combination of impedances Z_{g1} and Z_{g2}.

The results of GNC based stability analysis is shown in Figure 2.4 in red. Intersection of the characteristic loci with the unit circle is identified and a line L_1 is defined joining the origin with the intersection point. The phase margin (PM) is basically the angle subtended by line L_1 with the negative real axis. Two eigen values correspond to two different PMs. The minimum PM is taken as the final PM of the system [1]. Hence for Case 1, the PM is 33.02°.

Comprehending stability:

Let's consider Case 1. By observing the red contour for λ1 and λ2, the number of anti-clockwise encirclements around the critical point -1+j0 (denoted with a red star in Figure 2.4) is noted. Since there are no such encirclements, $\mathbf{N_1}=0$ and $\mathbf{N_2}=0$. The number of unstable poles ($\mathbf{P}$) of the MLG or $\mathbf{L}$ was found to be 0. Therefore, by applying the GNC from equations outlined in annex A.1, we get $\mathbf{Z}=0$. Thus, implying absence of unstable poles in the closed loop system.

Result: Closed loop system is stable.

2.2.2.2 Case 2: Highly damped case

The parallel combination of the impedances Z_{g1} and Z_{g2} form the net grid impedance. A similar analysis is presented for this case, the system is found to be stable with $\mathbf{Z}=0$. The phase margin however is 62.46° and it is obtained using the line L_2. A step change in *d*-axis current reference is applied from 200A to 300A, while maintaining the *q*-axis reference to zero. The oscillations are lesser compared to the previous case. The peak overshoot, undershoot and settling time are much lower compared to the previous case owing to higher stability margins as observed from Figure 2.5 and Figure 2.6.

2.2.3 Results

Stability of the system predicted by theory using GNC methodology is validated by time domain simulations. The phase margins provide an intuitive idea of robustness as we have shown that when margins are lower, the damping in the system is lower leading to oscillations. We have also shown that the phase margin is dependent on the grid impedance.

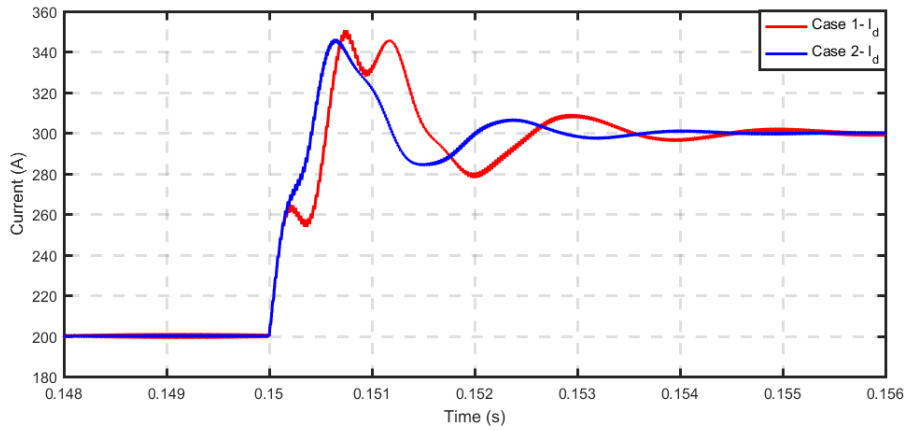

Figure 2.5 Comparison of Id step response (Id = 200A to 300A)

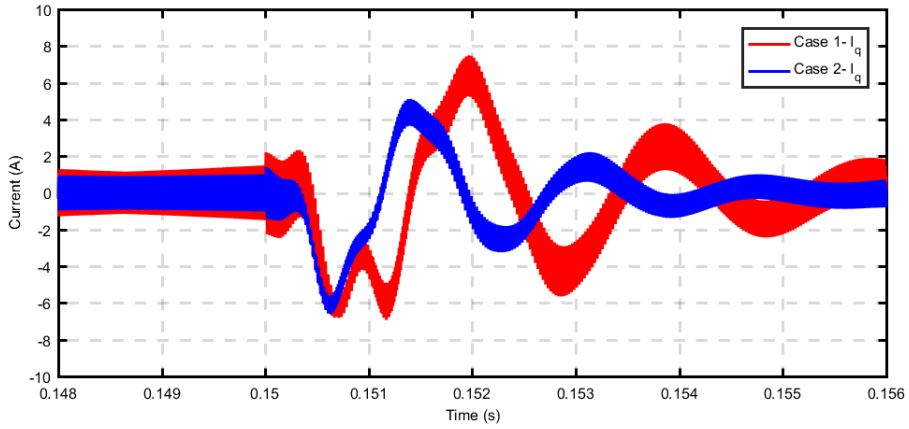

Figure 2.6 Comparison of I_q step response (I_d = 200A to 300A)

2.3 Impact of phase locked loop (PLL)

In this section, the impact of phase locked loop (PLL) on the system dynamics is studied. The PLL is a device which is used to provide synchronisation of the inverter output frequency and phase angle with that of the grid. The estimate on the phase angle obtained from the PLL is required for abc to dq conversion and vice versa.

2.3.1 PLL Modelling

The goal of PLL is to align the controllers synchronous reference frame (SRF) with the systems SRF. The objective of the PLL is to drive the q component of the voltage in the controllers SRF to zero. Analogous to the controller of the inverter, the PLL uses a PI controller whose output is the angular frequency and on feeding this signal to an integrator (denoted by 1/s in Figure 2.7), one obtains the phase angle θ which is used as a feedback. Therefore, the PLL is a closed loop control system as shown in Figure 2.7. The bandwidth of PLL has an impact on the measurement. Since an ideal PLL with infinite bandwidth is not possible, there is always a small error or difference in the estimate of the phase angle. The dq frame of the control system lags the dq frame of the inverter power stage by some angle $\Delta\theta$ as shown in Figure 2.7. Due to this effect, the measured current, voltages and thus the impedance is also affected due to PLL.

The SRF PLL as described above cannot suppress the double frequency ripple due to unbalance in grid voltages [9]. A decoupled double SRF (DDSRF) PLL solves the double frequency issue. However, considering the futuristic scenario, with algorithms such as Sv_B in place, the unbalance will be managed within stipulated limits and this implies that severe unbalances are out of context. Additionally, both SRF and DDSRF PLL exhibit a negative resistor like behaviour.

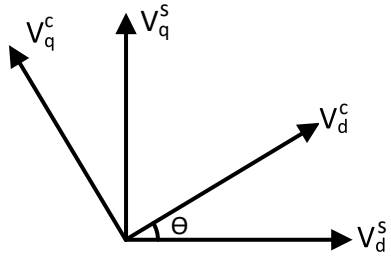

Influence of PLL on controller frame

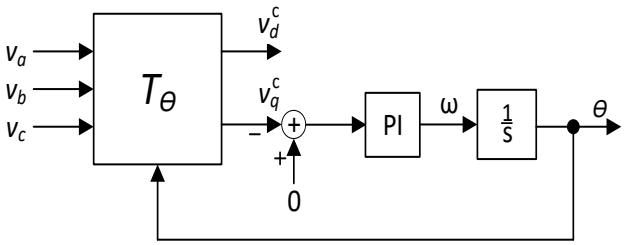

PLL Control System

Figure 2.7 PLL model

2.3.2 Modelling of grid connected inverters with PLL

The PLL dynamics impacts the current and voltages at various frequencies. The impedance in the channel *qq* (Z_{qq}) gets shaped as a negative resistor at low frequencies. In deliverable D3.1, the impact of a negative resistance behaviour attributed to presence of constant power loads (CPL) in the grid was explained. The destabilizing effects of CPL bandwidth can be found in [15], [16]. Analogously the impact of negative resistor like behaviour of the grid impedance in the *qq* channel due to the PLL has a destabilizing effect. The decoupling control present in the inverter can only minimize the cross-coupling impedances (Z_{dq} and Z_{qd}) between the *d* and *q* channels and does not modify the negative resistance behaviour of Z_{qq} in channel *qq*.

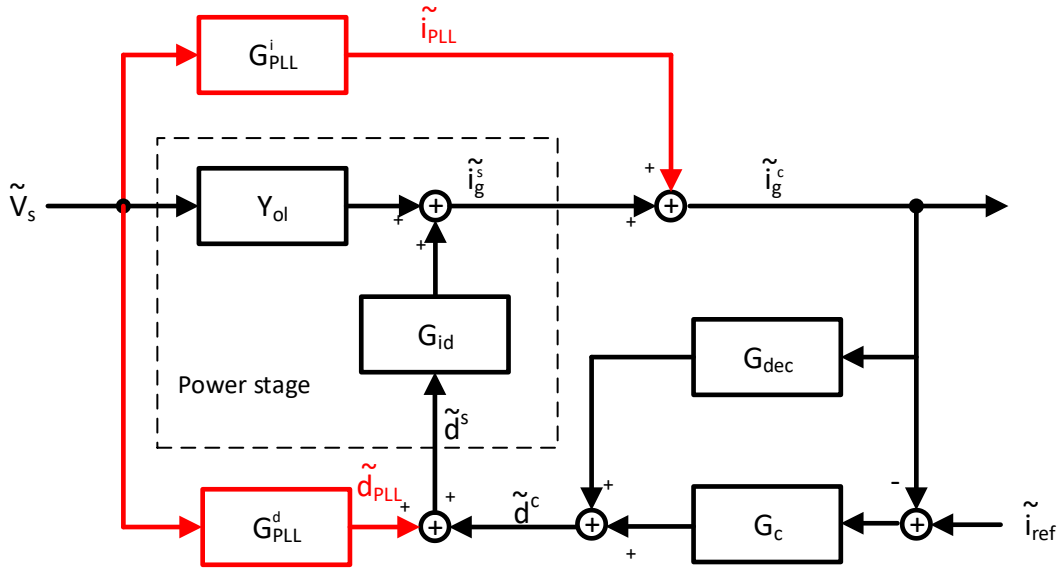

Figure 2.8 Impact of PLL

The PLL effect on the grid injection current i_g is denoted by the transfer function G^{i}_{PLL} which causes the additional current i_{PLL} to flow as shown in Figure 2.8 denoted by red line. Hence the measured current i^{c}_{g} is the sum of the actual grid feed current in inverter i^{s}_{g} and i_{PLL}. The duty cycle set by the controller is affected by the PLL through the transfer function G^{d}_{PLL} as shown in Figure 2.8 denoted by red line. The mathematical formulation of the PLL impact on the inverters output impedance is shown in the annex.

2.4 Extensions to an active grid

In this section, a description of the simulation test scenario is provided.

2.4.1 3 Node LV feeder description

The simulations are extended to the case of an active grid. The RES units are interfaced to the LVAC feeder through the inverter and each point of common coupling (PCC) is considered as a node. There will be about 10000 such PCCs per secondary substation automation unit (SSAU) and hence 10000 nodes. For simulation purposes, a 3-node feeder is considered. As shown in Figure 2.9 and Figure 2.10, based on the position of the switch S, the system would operate in either grid connected mode or in islanded mode (as a Microgrid).

2.4.2 Grid Connected Mode

In the grid connected mode as shown in **Error! Reference source not found.**, the switch S is in closed position enabling grid connection. The three inverters are operated in current control (CC) mode as denoted in figure. The control objective is to inject the current based on the set-points provided for the controller. To have control of the grid injection current, the inverters have a LCL filter at the output. The current measurement through the grid side L filter is used for feedback as shown in figure. A resistive load is present at the second node. From theory, the control parameters have an impact on impedance and thus on stability. Impact of controller gains on stability is presented in next section.

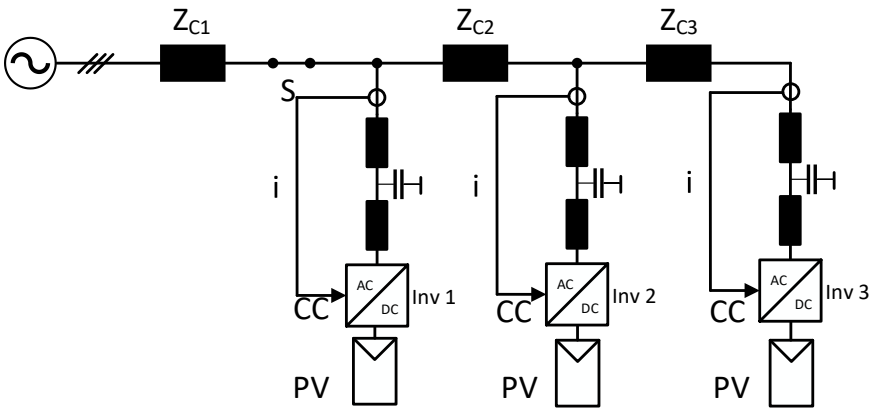

Figure 2.9 3-node LV feeder: Grid connected case

2.4.3 Islanded grid Mode

In the grid connected mode as shown in Figure 2.10, the switch S is in open position. Inverter 1 is operated in voltage control (VC) mode. An LC filter is used at the output of the inverter 1. The remaining two inverters are operated in current control (CC) mode like the previous case as denoted in figure. The effect of PLL and control parameters on stability is presented in the next section.

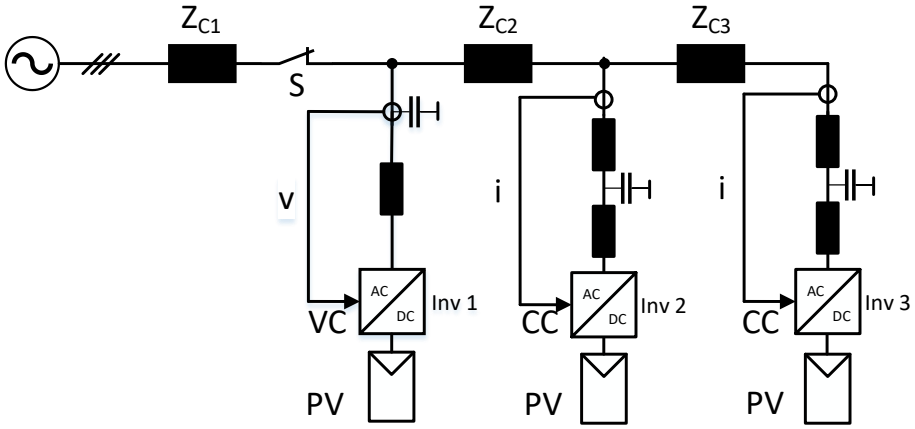

Figure 2.10 3-node LV feeder: Microgrid case

2.5 Stability analysis

This section performs stability analysis based on GNC for the 3-node LV feeder case. The impedance at every bus is calculated by applying Thevenin and Norton circuital theorems. The annex provides an example of impedance computation based on Thevenin and Norton theorems. Time domain simulations of the system are performed to validate the theoretical formulations.

2.5.1 Case 1: Grid connected mode

2.5.1.1 Stable operation of Inverter 1

A stable controller is designed based on the mathematical model of an inverter. Stability is analysed at every PCC and the corresponding characteristic loci is shown in Figure 2.11. The system is stable due to absence of open loop unstable poles and no encirclements of the characteristic loci around the critical point. A step change in the current reference is made from 30A to 10A for all 3 inverters. A stable response is observed for the grid injection current and the output voltage of the inverter as shown in Figure 2.12.

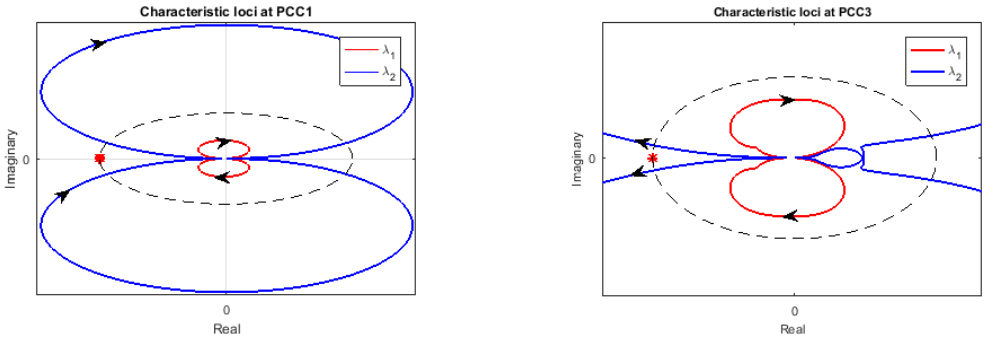

Stable node: PCC1 Stable node: PCC3

Figure 2.11 Grid connected mode: Stable case: Characteristic loci at PCC1 and PCC3

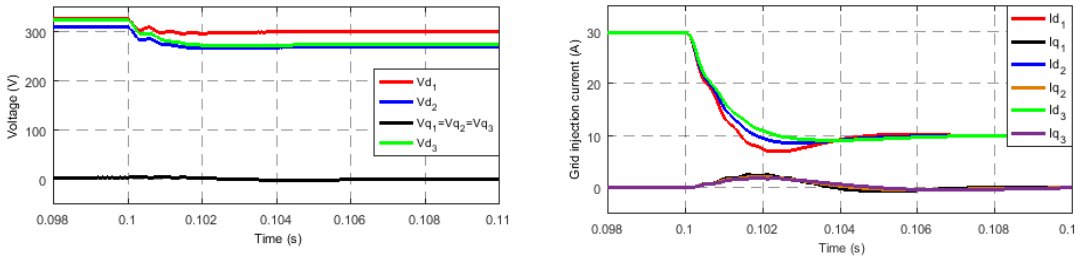

Bus Voltage Grid injection current

Figure 2.12 Grid connected case: Stable case: Inverter currents and voltages

2.5.1.2 Unstable operation of Inverter 1

The controller gains of Inverter 1 are increased to make it unstable, as suggested from the time domain simulations shown in Figure 2.13, where both voltage and current of Inverter 1 are unstable. The open loop transfer function evaluated at PCC1 contains unstable poles. The characteristic loci plot of this configuration as shown in Figure 2.14 shows the presence of closed loop unstable poles due to the absence of encirclements of the characteristic loci around the critical point. The currents and voltages of PCC2 and PCC3 are stable due to the stiff support from the grid. The open loop transfer function evaluated at PCC2 does not contain any unstable poles and as seen from Figure 2.14, there are no encirclements of the critical point. Hence there are no unstable poles in the closed loop system. Thus, the time domain simulations and the results obtained mathematically through GNC are in perfect agreement.

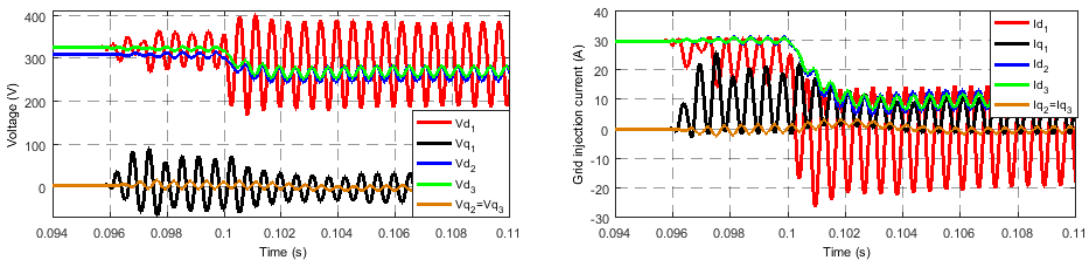

Bus Voltage Grid injection current

Figure 2.13 Grid connected mode: Unstable case: Inverter currents and voltages

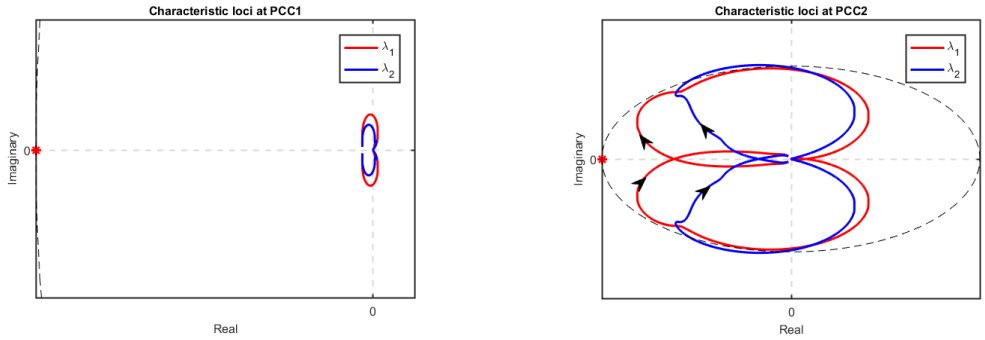

Unstable node: PCC1 Stable node: PCC2

Figure 2.14 Grid connected mode: Unstable case: Characteristic loci at PCC1 and PCC2

2.5.1.3 Result

The impedance of the inverter depends on the controller gains. The overall stability is a function of all the impedances in the system. Thus, one can infer that the controller gains have an impact on system stability. Validation of the above statement is obtained from the simulation results. Gain and phase margins are important small signal stability measures and these measures are key to defining new grid codes. In the next deliverable, detailed coverage will be provided on how stability margins can be used for defining grid codes.

2.5.2 Case 2: Islanded mode

In the islanded mode of operation, Inverter 1 solely provides voltage support. Inverter 2 and 3 acts as current sources, i.e they inject currents based on the set-points provided by the power controller. Like simulation test case 1, the control parameters have an obvious impact on the grid voltage stability. However, the PLL gains have a critical impact on stability due to the negative resistor like behaviour of the *qq* channel impedance. It is therefore of interest to perturb the PLL gains as the inverter operates and observe the grid voltages and currents.

2.5.2.1 Stable case

The inverters are operated with stable values of the PLL gains until a stable steady state is reached. At time t = 0.05s, a change in the PLL gains of Inverter 2 and 3 are implemented. This change basically increases the bandwidth of the PLL. A sudden increase in the frequency of Inverter 2 and 3 are observed as shown in Figure 2.17 during this time instant. However, due to a stable impedance configuration as determined using the GNC, the frequency restores back to 50 Hz. The currents and voltages are plotted in Figure 2.15 where the stable response is shown. The voltages and currents reach their new steady state values in 0.005s.

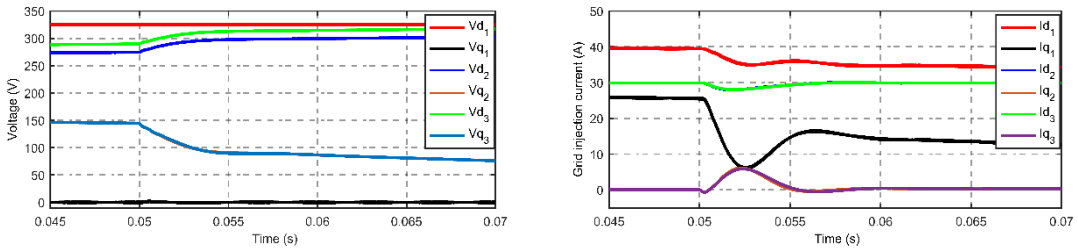

Bus Voltage Grid injection current

Figure 2.15 Islanded mode: Stable case: Inverter currents and voltages

2.5.2.2 Unstable case

When the PLL bandwidths of current controlled Inverters 2 and 3 are sufficiently reduced, the PLL cannot successfully track the normal 50Hz sinusoidal voltage. In this case, the frequency drops abruptly and does not restore back as shown in Figure 2.17. The wrong data of the angle given by the PLL impacts the voltages and currents in *dq* domain that are used for control purposes. Hence, the grid voltages and current begin to collapse and oscillate as shown in Figure 2.16. The grid is operating in an unstable mode.

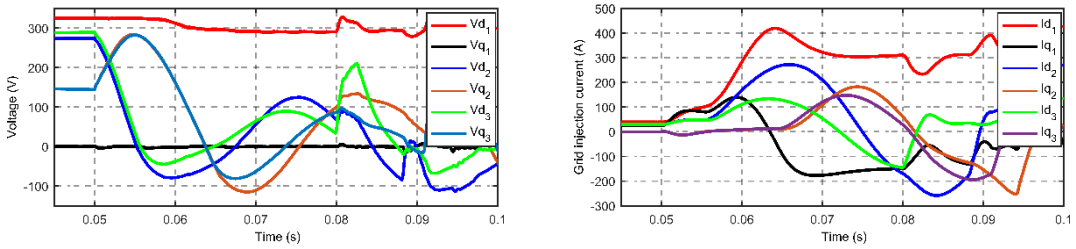

Bus Voltage Grid injection current

Figure 2.16 Islanded mode: Unstable case: Inverter currents and voltages

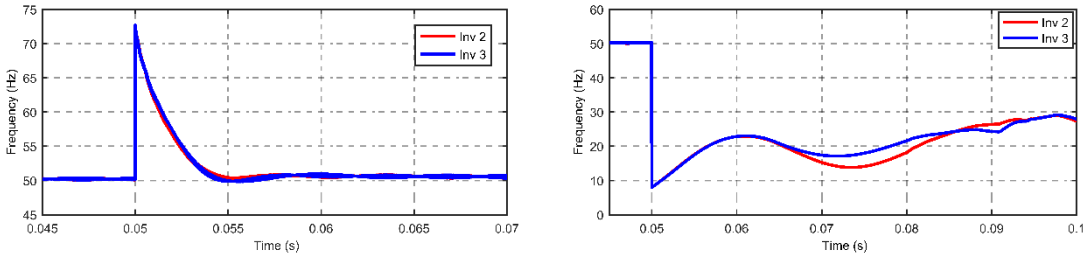

Stable case: PLL bandwidth increased Unstable case: PLL bandwidth decreased

Figure 2.17 Frequency response comparison for stable and unstable PLL configurations

2.5.2.3 Result

The impedance of the inverter also depends on the PLL gains. The overall stability is a function of all the impedances in the system. Thus, one can infer that the PLL gains have an impact on system stability. Validation of the above statement is obtained from the simulation results. Stability of the system depends on the stability inverters and stability of loads. In this deliverable, passive loads such as RLC loads were considered, which are stable. But in future deliverables, active rectifiers will be considered which act as a nonlinear load (constant power load).

2.6 Conclusion and future work

This deliverable performs validation of the GNC concept with a single grid connected inverter, where the PLL dynamics were ignored. The stability analysis of this rather simple case shows how the grid impedance can affect the stability margins of the system.

The impacts of PLL dynamics were modelled and its impacts on the inverter impedance was studied. The PLL basically impacts the duty cycle and the observed current. The net effect is that the *qq* channel impedance gets shaped as negative resistor. Extension of the GNC for a grid scenario was provided in this deliverable by the consideration of an exemplary 3-node LV feeder. The impacts of the control parameters and PLL gains on stability were analysed through GNC and verified through time domain simulations.

The future deliverables will consider active rectifiers in the grid. Since DC loads are unavoidable in the future, stability analysis of the fast dynamics of active rectifiers need to be addressed. A

3-node LV feeder will be considered with the presence of active rectifiers and GNC will be applied followed by time domain simulations. Hardware in the Loop (HiL) will be introduced to identify impedances in real time. Furthermore, Power Hardware in the Loop (PHiL) simulations are also planned and will be subjected to deliverables.

3. Voltage management using inverter-based RES units

This Chapter presents the active regulation of voltages using inverter-based RES on a sample section of a real LV distribution network with representative customer connections. The assumptions emphasised in **D3.1** serve to highlight the complexity of achieving a complete solution to voltage control on LV feeders hosting RES. The interaction of the customer load with the local observed voltage, while causing differing effects dependant on the ZIP[1] composition, is perhaps the best indicator for the overall health of the voltage profile of a feeder. The Active Voltage Management (AVM) technique builds upon the work of [17] to implement a decentralised voltage control concept that can be readily put to trial in **WP5**.

This chapter reveals the extent to which ZIP demand modelling is used for the creation of a multi-scenario analysis, details the aspects of the 3-OPF modelling tool, derives volt-var curves for the two potential objectives of a DSO (namely, minimisation of voltage unbalance and minimisation of active power losses) and finally, presents a walkthrough of the AVM technique by use of a case study.

3.1 The Active Voltage Management Technique

The AVM technique is a decentral approach to voltage control for maintaining steady state voltage in the presence of RES. The technique capitalises on the inverter-based RES units by engaging with the provision of reactive power from these units.

The AVM technique consists of a multi-scenario three-phase AC OPF analysis of RES connections on LV feeders. An offline network analysis takes place, which is a centralised solution that determines:

- an optimal voltage set-point for each point of RES connection
- the range of expected voltages anticipated at the point of connection
- the spread of reactive power set-points that would render the RES connection capable of achieving the voltage target
- objective governed volt-var curves for online *decentral* deployment

The output of this **offline** network analysis is a prescribed volt-var curve per RES connection determined while fulfilling a single objective of the network operator. The procedure can be repeated to satisfy any objective of the DSO that can be formulated within feasible conditions of an AC OPF. In the field, and in further time-series simulation, these volt-var curves dictate the voltage control at each point of connection of a RES by utilising the inverter capabilities. The only required input for corrective action to take place is the voltage magnitude measurement local to the RES unit.

3.2 Multi-Scenario ZIP Diversification

On LV networks, the consideration of *voltage sensitivities* is of utmost importance. Voltage sensitivity is a product of the physical infrastructure the network embodies but is also dependent on the generation and load composition. As identified in **D3.1**, proposed solutions for accommodating RES on LV feeders must account for these affects.

A bottom-up demand model [18] is used here to construct a representative demand profile of any amount of customers on an LV feeder. This model epitomizes occupancy patterns and behavioural characteristics of the customer to provide a load composition that gives an accurate representation of the devices assumed to be drawing current. Thus, this style of model has the advantage of also including the representative ZIP composition of the customer premises. By extension, the use of these components will reveal the inherent voltage sensitives of these networks that will align with that of a physical LV feeder.

[1] ZIP composition refers to the compartmentalisation of demand as constant impedance, constant current and constant power.

Discerned from this input are points of interest (POI) that are passed to the offline optimisation procedure, to be analysed all at once in what is known as a **multi-scenario** OPF. In the case of the test feeder used for simulations of **D3.2**, 74 customers are assigned a demand profile from the bottom-up demand model. The profile of the total active power drawn at the head of the feeder, where the SSAU is to connect, is seen in Figure 3.1 for a period of 24 hours and with a resolution of 1 minute.

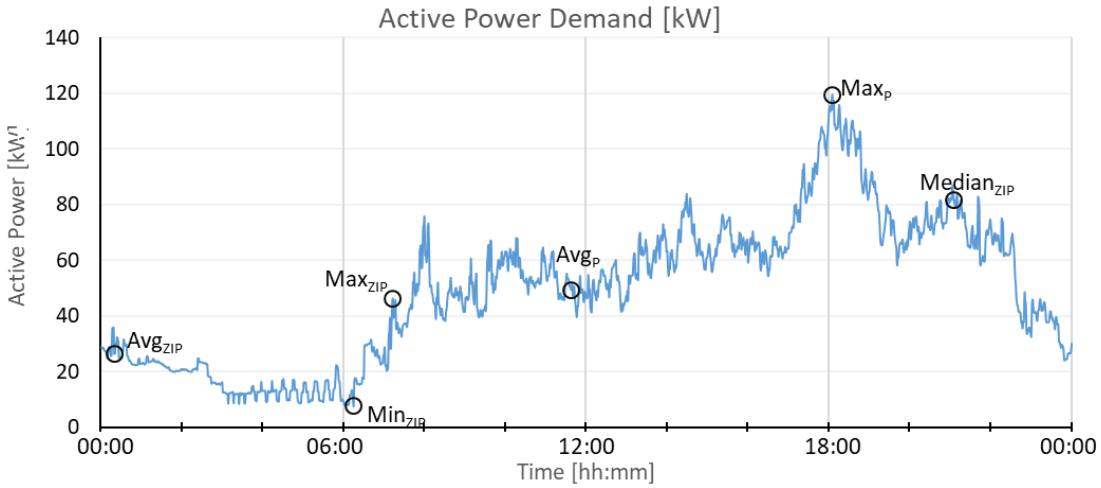

Figure 3.1 Active power demand of 74 customers supplied to LV feeder identifying POI

Also seen in Figure 3.1 are points of interest (POI) identified for use in the multi-scenario three-phase OPF to follow. The POI represent the maximum, minimum and average active power demand; denoted Max_P, Min_P and Avg_P respectfully. Note that in this instance the Min_P point is shared with the Min_{ZIP} point. The active power P_d and reactive power Q_d drawn at a particular customer premises becomes a function of voltage and the active power rating, P_O, and reactive power rating, Q_O. This formulation is represented by equations (3.1) and (3.2):

$$P_d = P_O\left(Z_P\left(\frac{V}{V_O}\right)^2 + I_P\left(\frac{V}{V_O}\right) + P_P\right) \tag{3.1}$$

$$Q_d = Q_O\left(Z_Q\left(\frac{V}{V_O}\right)^2 + I_Q\left(\frac{V}{V_O}\right) + P_Q\right) \tag{3.2}$$

where, V is the voltage at the customer premises, V_O is the nominal voltage, Z_P and Z_Q are the constant impedance component for active and reactive power, I_P and I_Q are the constant current components for active and reactive power, P_P and P_Q are the constant power components for active and reactive power of demand.

The remaining POI are more clearly identifiable in Figure 3.2, where the aggregate ZIP composition exponent for the feeder has been extracted from the bottom-up demand profile modelling. These POI represent the maximum, minimum, average and median ZIP exponent compositions; denoted Max_{ZIP}, Min_{ZIP} and Avg_{ZIP} and $Median_{ZIP}$ respectfully.

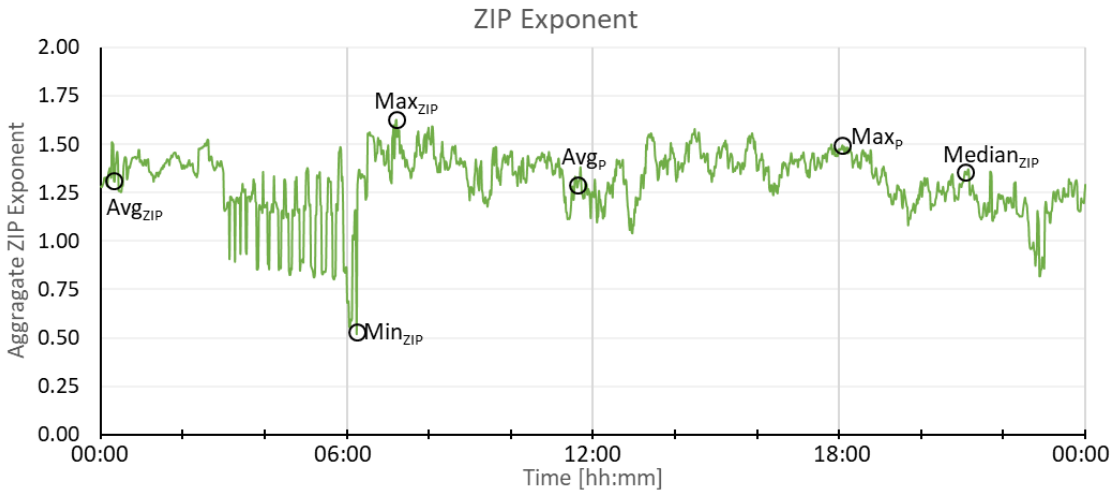

Figure 3.2 Aggregate ZIP composition of 74 customers identifying POI

Figure 3.2 shows the aggregate ZIP load composition of the 74-customer feeder. As seen the scale of this axis is within the range of *zero* to *two* and varies over the course of a 24-hour period. Equation (3.3) equates the aggregate ZIP composition exponent, where the ZIP composition for each house has been calculated and summed in equation (3.4) to obtain the aggregate ZIP composition for a given time step.

$$\eta_P = \frac{Z_{agg}(2) + I_{agg}(1) + P_{agg}(0)}{Z_{agg} + I_{agg} + P_{agg}} \tag{3.3}$$

$$\begin{bmatrix} Z_{agg} \\ I_{agg} \\ P_{agg} \end{bmatrix} = \sum \frac{P_d}{P_{agg}} \begin{bmatrix} Z_d \\ I_d \\ P_d \end{bmatrix} \tag{3.4}$$

As indicated by the formulation of equation (3.3) an η_P value of *two* indicates that the all households on the feeder have purely constant impedance load, whereas a value of *one* is indicative of a constant current load and a value of *zero* represents the case where every household is drawing a load of constant power. The POI of interest identified for analysis in the multi-scenario OPF accounts for the variation in voltage sensitivities that are concurrent with these ZIP component cases. Solutions obtained in an OPF setting accommodate the wide-ranging effects the diversified loads contribute to the management of voltages and feeder thermal constraints.

3.2.1 Generation Profiles

The simulations conducted here considers the connection of PV inverters. The resulting power flows with active power generated from these units is examined from 0 – 100% output in increments of 25%. So, for a 2 kW installation, 0, 0.5, 1, 1.5 and 2 kW outputs are examined. These snapshot generation points combine with the POI identified for the ZIP composition of demand to create the multi-scenarios used for simulations by the 3-OPF tool in the offline modelling phase. This reduces what could have been an extensive computational burden to just **35 scenarios** for analysis in the 3-OPF tool.

In section 3.4, the online deployment phase, a week-long period is investigated whereby historic generation profiles from solar PV installations are used with the volt-var curves calculated as the output of the AVM technique.

3.3 3-OPF modelling tool

The AVM technique requires the analysis of multi-scenario AC OPF, the chosen tool for this task is the 3-OPF tool, created within the Energy Institute at UCD. The 3-OPF tool employs a mathematical technique (*or solver*) to navigate the solution space outlined by the problem set formulated from the expressions in (3.5) - (3.7). A converged solution ought to satisfy the equations governing power flow and once achieved a steady-state operating point is guaranteed.

Figure 3.3 gives an overview of the typical work flow of the 3-OPF tool. A database is used to store the parameter values, such as the topology of the network, known demand profiles and ZIP components; these are fed into the 3-OPF to specify the initial conditions. On completion of the simulation the results are fed back to a database, where there is an opportunity to update parameter values for the next iteration and store variable quantities, such as, calculated voltages, resulting current flow and required reactive power settings.

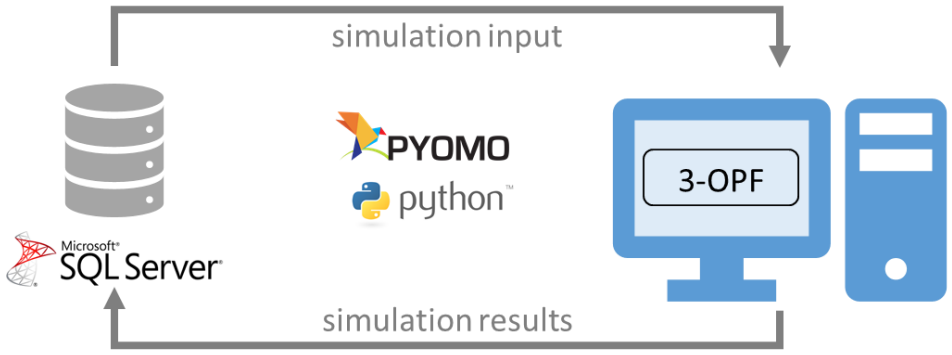

Figure 3.3 Workflow of the 3-OPF modelling tool

Optimal Power Flow

A general optimisation problem is expressed in (3.5) - (3.7), here the constraints of an AC OPF formulation reside.

$$\min_{X} f(X) \tag{3.5}$$

$$H_n(X) \leq 0, n \in \Gamma_{ineq} \tag{3.6}$$

$$G_m(X) = 0, m \in \Gamma_{eq} \tag{3.7}$$

where, Γ is the set of all constraints, *H* and *G* are the set of inequalities and equalities for the variables *X*. The expression of quantities in this manner provides the means to explore any desired decision variable and express countless objective functions. The full list of variables and parameters used by the 3-OPF platform are provided in Table A.2.1 of annex A.2.

The 4-conductor current flow approach [11] is used to formulate the OPF problem. With this approach, the power generated, transferred or consumed by the equipment at each bus and phase in the network is converted to current components. The constraint responsible to achieving realistic and representative power flow results are those defining Kirchoff's Current Law, which states that net current flow into a node must equal zero. This theory is embodied in the 3-OPF tool in *real* and *imaginary* current components, found in equation (3.8) and (3.9) respectively. A complete explanation of parameters and variables is provided in Table A.2.1 of annex A.2.

$$\sum_{g=1}^{G} \mathrm{Re}\{I_g\}_{b,\varphi} = \sum_{d=1}^{D} \mathrm{Re}\{I_d\}_{b,\varphi} + \sum_{l=1|_{\varphi=\rho}}^{L} \mathrm{Re}\{I_{l,\rho}\}_b \tag{3.8}$$

$$\sum_{g=1}^{G} \mathrm{Im}\{I_g\}_{b,\varphi} = \sum_{d=1}^{D} \mathrm{Im}\{I_d\}_{b,\varphi} + \sum_{l=1|_{\varphi=\rho}}^{L} \mathrm{Im}\{I_{l,\rho}\}_b \tag{3.9}$$

As identified in **D3.1**, the branch ampacity, and node voltage bounds are to be upheld on the convergence toward a feasible solution. Equation (3.10) defines an inequality to constrain the current on a branch, l, and phase, φ to be below the known current limit.

$$\left|I_{l,\varphi}\right| \leq I^{+}_{l,\varphi} \tag{3.10}$$

Similarly, the inequality of equation (3.11) formulates the requirements to constrain the voltage magnitude of the nodes on the system within known operating limits.

$$V^{-} \leq \left|V_{b,\varphi}\right| \leq V^{+} \tag{3.11}$$

3.3.1 Determination of the volt-var curves

A four stage multi-scenario analysis, building on the work of [17], is used to investigate the volt-var curves that arise from differing objectives of the DSO. An initial objective chosen to showcase the methodology is **the minimisation of voltage unbalance**, is discussed below.

The selection of multiple-scenarios is further explained in section 3.2. These scenarios represent a range of aggregate ZIP compositions that would be anticipated during a single day, combined with a range of active power generated by a RES. In multi-period analysis, a natural trade-off is determined in a single scenario for the good of all scenarios considered.

The network topology, impedance information and the active and reactive power settings of demand customers and RES alike are represented in a database. This database is fed to the 3-OPF tool in **Stages I – IV** for the formation of the volt-var curves.

3.3.1.1 Stage I – Optimal voltage setting

The purpose of Stage I is to ascertain the single optimal voltage at the terminals of the RES connection that optimises the object function across the multi-scenario case study. As stated, in this case study, the objective is defined as the minimisation of voltage unbalance, as formulated in equation (3.12):

$$\begin{aligned} &\min \quad f \\ &f = \sum_{s\in Sc}\sum_{b\in B}\sum_{\varphi\in\Phi} \mathrm{Vunb}_{s,b,\varphi} \end{aligned} \tag{3.12}$$

where Sc is the set of all scenarios and B is the set of all buses and Φ is the set of all phases. In a single scenario, the model calculates the voltage unbalance (for a bus b, phase φ) from equation (3.13), which is the difference between the voltage magnitude on a phase, $V_{b,\varphi}$, and the average bus voltage, $\overline{V}_b^{abc}$, as a fraction of the average bus voltage.

$$\mathrm{Vunb}_{b,\varphi} = \frac{V_{b,\varphi} - \overline{V}_b^{abc}}{\overline{V}_b^{abc}} \tag{3.13}$$

Critically, the voltage achieved at the terminals of a RES in the multi-scenario OPF analysis should be the same across all scenarios, this equality constraint is provided in (3.14).

$$\mathrm{Vopt}_{b,\varphi} = \mathrm{V}_{s,b,\varphi} \qquad \forall s \in \mathrm{Sc}, \quad b \in \mathrm{RES} \tag{3.14}$$

Notably any objective could be formulated in place of equation (3.12) in Stage I of the analysis, for example the maximisation of reactive power support or minimisation of feeder active power losses, to name just two examples. This capability equips the DSO with achieving multiple objectives, at their discretion, by utilising the reactive power capabilities of the inverter-based RES on distribution system.

In Stage I, the reactive power resource available from the inverter technology is left unconstrained. The RES units are given more than enough headroom to operate within, a range of [-15, 15] kVAr. Examining the output from 0 – 100% rated active power usage of the RES in the multi-scenario of demand provides a single voltage magnitude per RES unit. The **voltage magnitude** found here for each RES is passed to Stage II of the analysis.

3.3.1.2 Stage II – Minimal voltage deviation

Taking the voltage target output ($\mathrm{Vopt}_{b,\varphi}$) from Stage I, Stage II determines, for every scenario, the minimal possible voltage deviation from optimal. A change in objective function formulation is required here, this objective formulation is found in (3.15):

$$\min \quad g$$
$$g = \sum_{s \in Sc} \sum_{b \in RES} \sum_{\varphi \in \Phi} (\mathrm{V}^2_{s,b,\varphi} - \mathrm{Vopt}^2_{b,\varphi})^2 \tag{3.15}$$

The new objective minimises the difference in the sum of squares between the optimal target voltage and the best possible voltage achievable by utilising the available reactive power. For Stage II of the analysis, the reactive power constraints of the RES are implemented. In the case of inverter capabilities of a PV, there is a limitation in the amount of reactive power resource the device can provide, directly proportional to the active power output. This is typical of inverter-based technologies. Figure 3.4 shows the capability chart of a generic PV system, illustrating the bounds of reactive power supply shown as the active power of the unit increases from zero to maximum output, P^{+}_{res} .

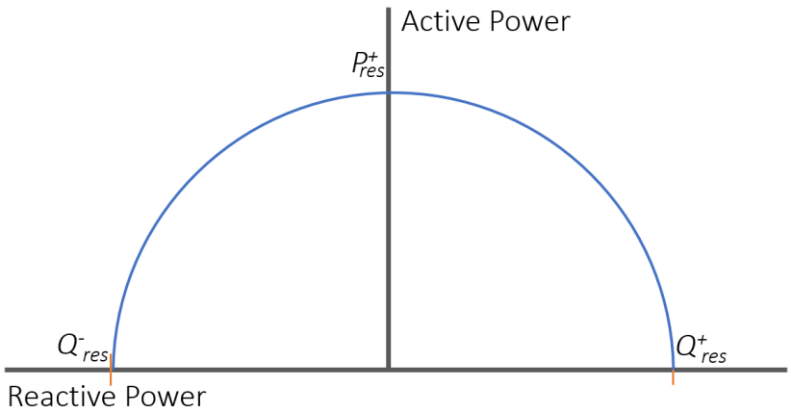

Figure 3.4 P-Q capability chart of a generic PV system

Mathematically, this limitation on reactive power is expressed with the use of the inequalities in equation (3.16) and (3.17):

$$\mathrm{Q}^{-}_{s,res,\varphi} \geq -\sqrt{(\mathrm{S}_{res,\varphi})^2 - (\mathrm{P}_{s,res,\varphi})^2} \tag{3.16}$$

$$Q^{+}_{s,res,\varphi} \leq \sqrt{(S_{res,\varphi})^2 - (P_{s,res,\varphi})^2} \tag{3.17}$$

$$Q^{-}_{s,res,\varphi} \leq Q_{s,res,\varphi} \leq Q^{+}_{s,res,\varphi} \tag{3.18}$$

In Stage II, the reactive power of the RES unit is left as a decision variable to operate within the bounds of (3.18). These equations are implemented in the 3-OPF tool and the optimisation procedure is run once for each inverter-based RES connection to be fitted with a volt-var curve. The **reactive power set-points** of Stage II, obtained for each RES, are stored to be used as one of two inputs to Stage IV.

3.3.1.3 Stage III – Representative voltage calculation

In Stage III, straightforward power flow solutions are obtained, with the RES constrained to operate at unity power factor. No optimisation is performed in this examination of the scenarios. The aim here is to examine the resulting voltages, should no reactive power be injected or absorbed at the location of RES. This analysis gives an indication of the representative voltages that may exist at varying generation levels coinciding with the voltage sensitivities of demand at these times. For this purpose, an additional constraint is required for Stage III to replace the inequality constraints of (3.16) - (3.18).

In equation (3.19), the equality constraint ensures unity power factor is observed at the terminals of the RES units.

$$Q_{s,res,\varphi} = 0 \tag{3.19}$$

The resulting **voltage magnitudes**, observed in each scenario, at the terminals of the RES units are the second and final input required to calculate the volt-var curves, in Stage IV.

3.3.1.4 Stage IV – Formulation of volt-var curves using linear regression

In Stage IV, the resulting reactive power set-points of Stage II and voltage set-points of Stage III, obtained for each RES under examination, are inspected to be formulated into a volt-var curve. Figure 3.5 shows an example of a volt-var curve. As seen the orientation of the volt-var curve should exhibit a negative slope and the intercept of the curve should match the optimal voltage set-point for the RES unit. The **slope** and **intercept** are the two characteristics to be determined from this offline analysis.

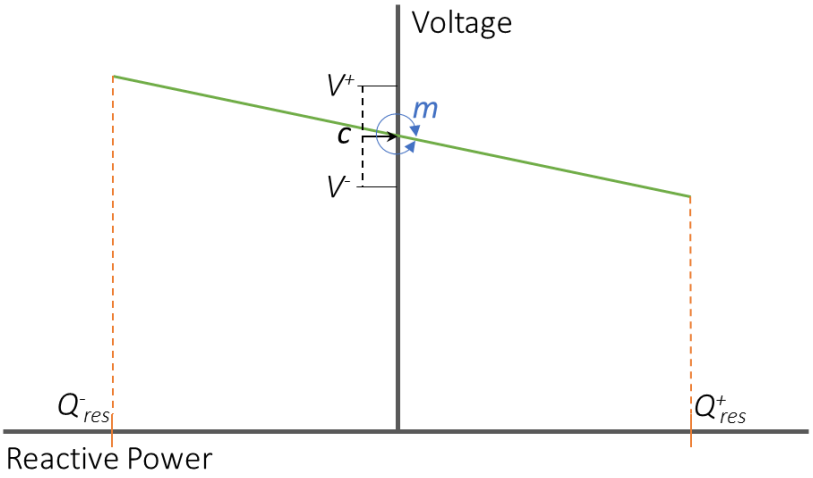

Figure 3.5 Sample volt-var curve showing orientation and bounds of voltage and reactive power

The intercept, c, of the volt-var plots should, in theory, match the exact voltage found for the RES systems in Stage I of this procedure. The slope of these curves (m, coefficient of Q_{RES})

guide the RES unit to control their absorption/injection of reactive power based on the monitored voltage at their terminals. Employing a linear regression analysis to the voltage and reactive power set-points, calculates the slope and intercept for each RES system. This formulates the relationship between the voltage observed at the terminals of the RES system, V_{RES}, to a reactive power output Q_{RES}, of the form seen in equation (3.20).

$$V_{RES} = mQ_{RES} + c \tag{3.20}$$

Recall, that in achieving the voltage, determined in Stage I, the RES units are providing sufficient reactive power to support, and achieve, the objective of the DSO; in this case the minimisation of voltage unbalance. Hence, the instructions can be relayed in a decentral manner for online-implementation of the AVM technique. A case study is performed in section 3.4 detailing the results of Stage I-IV as well as a time-series analysis of the resulting volt-var curves at work.

3.3.2 Summary

To summarise the procedure involved in producing the volt-var curves the following flow-chart of Figure 3.6 is provided.

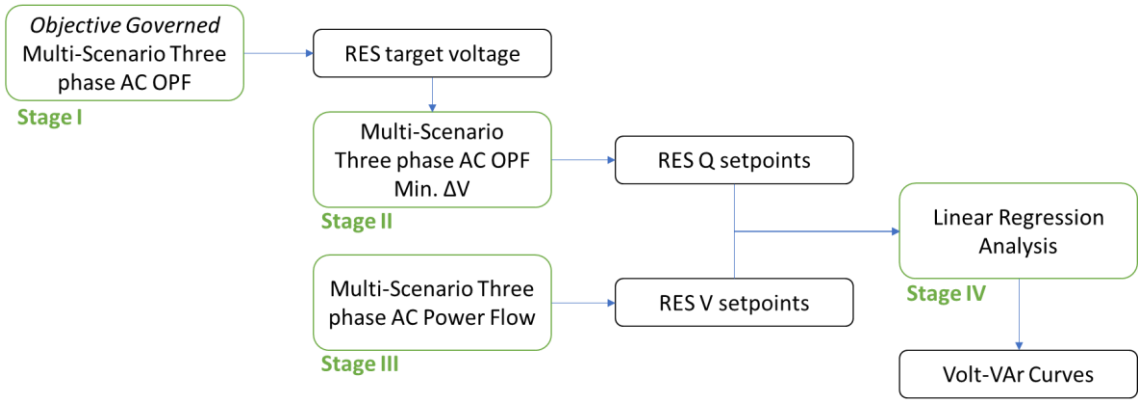

Figure 3.6 Procedure to determine objective governed volt-var curve using the 3-OPF modelling tool

- Stage I determines the optimal voltage across all scenarios that minimises the voltage unbalance of the feeder, or other objectives of interest.
- Stage II then determines the closest possible voltage deviation from optimal in each scenario, constraining the reactive power of the RES units to within representatively realistic bounds.
- In Stage III, the voltages are determined that occur at varying generation levels coinciding with the voltage sensitivities of demand at these times.
- Finally, to conclude the offline-procedure the resulting reactive power set-points (Stage II) are plotted against the resulting voltage set-points (Stage III) to determine the volt-var curves for each RES system.

The AVM technique reduces the *offline centralised analysis* to an *online and decentral deployment* through the means of optimally chosen volt-var curves, giving a practical means to facilitate the objectives of the DSO by managing the voltages on distribution systems. In section 3.4, the offline procedure is followed for a real LV test feeder and further time-series simulations are conducted as a proof-of-concept.

3.4 Case Study

A case study is presented in this section that features the analysis of two objectives of use to a DSO with RES connections on LV feeders. These two objectives are the **minimisation of voltage unbalance** across the 3-phase feeder and **active power loss minimisation** of the feeder. A common network is presented to simulate both objectives. Multiple scenarios are

discerned from the analysis of ZIP aggregate demand models for 74 customers, as per section 3.2. Using the 3-OPF modelling tool, the procedure to produce the volt-var curves is followed. To showcase the AVM approach operating in a simulation environment, time-series power flows are conducted where a comparison to a base scenario is made.

3.4.1 Network

The chosen network to showcase the AVM technique, and determine the volt-var curves for a series of RES, is a radial LV feeder with 85 nodes. The LV feeder is situated in Ireland and has been used for various network studies ([18]–[24]). The feeder steps down from a 10 kV network via a 10 kV to 400 V and 400 kVA transformer, assumed to be operating with a fixed tap. An underground cable, serving 11 three-phase supply nodes, distributes power via single-phase connections to 74 customers. Figure 3.7 illustrates the network topology with colour-coded phase connections for all 74 customers.

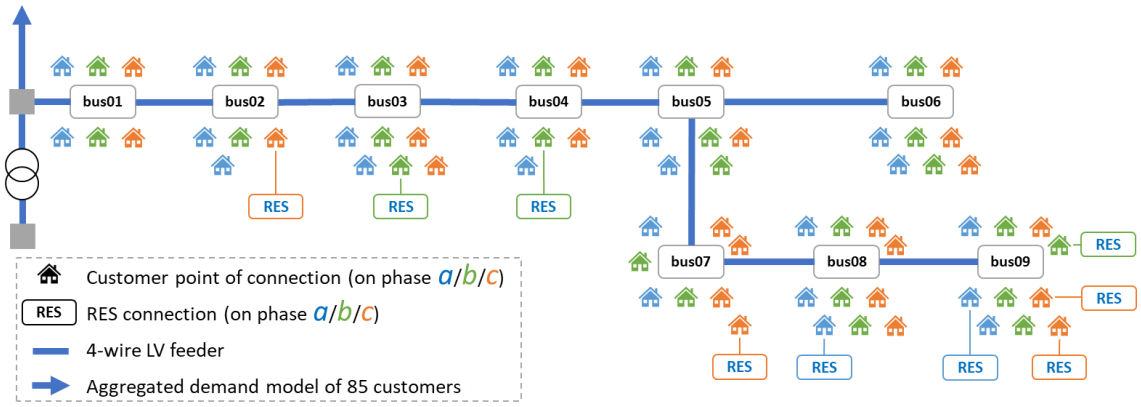

Figure 3.7 Network topology showing customer point of connection, phase and RES location

As shown on Figure 3.7, the presence of a further 85 customers are also included as a separate feeder connection off the transformer, representing another residential street of houses. This is done to ensure realistic voltage perturbations are observed at the head of the feeder in the multi-scenarios. The RES under analysis in this case study are inverter-based 2 kW photo-voltaic (PV) systems. Nine of these PV systems are represented in the 3-OPF model, connected to south-facing residential rooftops. The phase of these connections, location and three-phase supply node are displayed in Table 3.1.

Table 3.1 Location, phase, three-phase supply node and capacity of RES connections

RES	Location	Phase	Three-phase supply	Capacity
1	bus68	*a*	bus08	2 kW
2	bus81	*a*	bus09	2 kW
3	bus27	*b*	bus03	2 kW
4	bus35	*b*	bus04	2 kW
5	bus85	*b*	bus09	2 kW
6	bus19	*c*	bus02	2 kW
7	bus63	*c*	bus07	2 kW
8	bus76	*c*	bus09	2 kW
9	bus78	*c*	bus09	2 kW

The 4-wire (3-phase and neutral) LV feeder is modelled as a 4-core NAKBA 4x70 underground cable and the single-phase connections are assumed to be AYCY 1x25/16. In annex A.2, Table A.2.2 provides the series resistance, series reactance, shunt conductance and shunt susceptance properties by cable type for each node-phase pairing of the sample network.

3.4.2 Offline Modelling - Calculation of Volt-var curves

The offline modelling phase is repeated for two objectives of potential interest to a DSO with many RES connects on LV distribution feeders. These objectives are the minimisation of voltage unbalance and the minimisation of active power loss.

3.4.2.1 Minimisation of Voltage Unbalance

The objective function found in equation (3.12), is used in Stage I to determine the optimal voltage across all scenarios that **minimises the voltage unbalance** of the feeder. Stage II then determines the closest possible voltage deviation from optimal in each scenario, constraining the reactive power of the RES units to within representatively realistic bounds. In Stage III, the voltages are determined that occur at varying generation levels coinciding with the voltage sensitivities of demand at these times. Finally, to conclude the offline-procedure for this objective function, the resulting reactive power set-points are plotted against the resulting voltage set-points to determine the volt-var curves for each RES system. Table 3.2 presents the results of Stages I-IV producing the following characteristics for the RES connections under examination.

Table 3.2 Optimal voltage set-point, slope and intercept of RES systems for minimal voltage unbalance

RES	*m* [pu]	*c* [pu]	*Vopt* [pu]	Rel. Error [%]
1	-0.0148	0.9836	0.9842	0.03
2	-0.0179	0.9789	0.9774	-0.16
3	-0.0088	0.9957	0.9968	0.11
4	-0.011	0.9866	0.9808	-0.59
5	-0.0171	0.9790	0.9765	-0.25
6	-0.0045	0.9938	0.9900	-0.39
7	-0.0099	0.9894	0.9830	-0.65
8	-0.0119	0.9889	0.9800	-0.90
9	-0.0118	0.9888	0.9798	-0.92

As seen, the slope (m) from the volt-var curves are wholly negative, a sure indication that the AVM technique will inject reactive power when the measured voltage is below the target voltage and absorb reactive power while the measured voltage is above the target voltage. This is as expected as, under steady-state and stable operation, an injection of voltage will have the effect of raising the voltage magnitude at that location. Likewise, a reactive power sink will have the effect of reducing the voltage magnitude. The target voltage (intercept c) closely matches the optimal voltage ($Vopt$) determined with a generous allocation of reactive power capacity. In no case does the relative error between the intercept of the slopes and the $Vopt$ for each PV system exceed 1%. This indicates that under realistic conditions, where the reactive power capacity of the RES units is dependent on the active power (as modelled in Stage II), the target voltage can be achieved through the harmonious use of the reactive power at source.

Seen in sub-plots of Figure 3.8 are the reactive power set-points from Stage II and the voltage set-points from Stage III for each respective RES system.

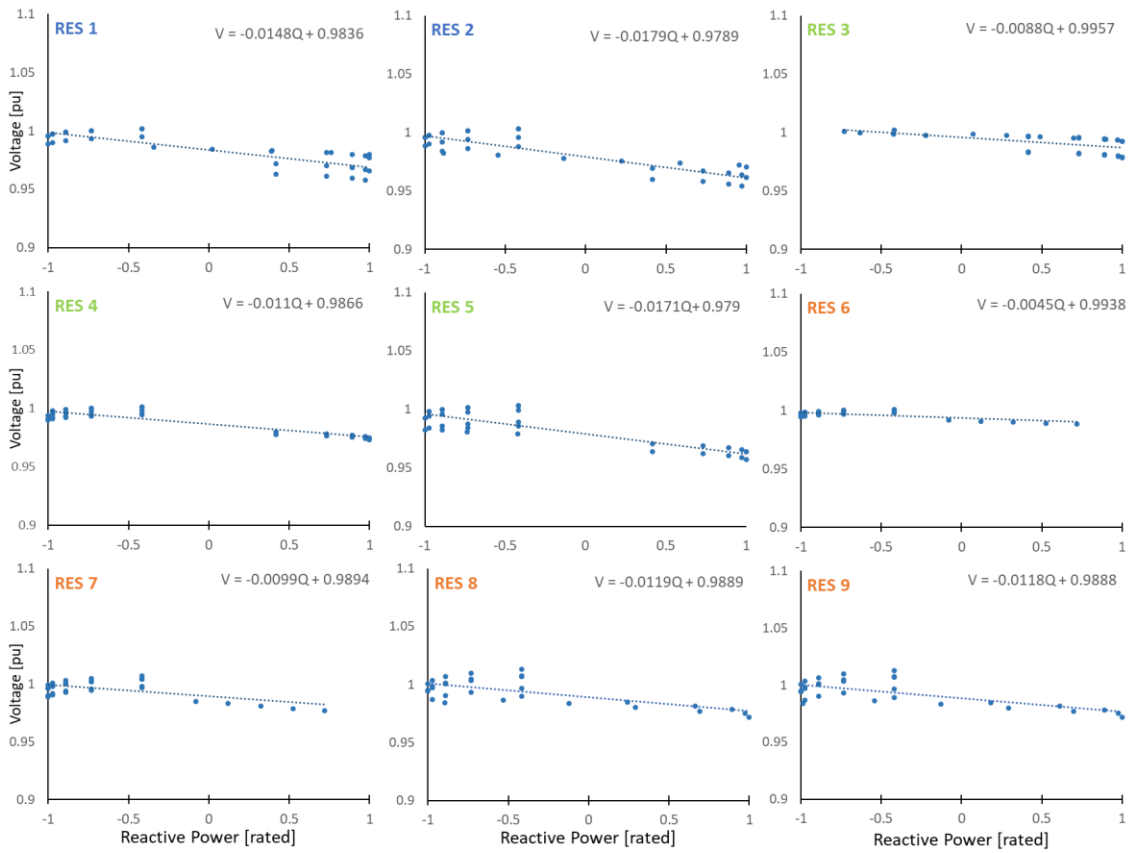

Figure 3.8 Resulting volt-var curves found for the minimisation of voltage unbalance for RES units 1-9, showing optimal voltages and slopes

In each subplot, the equation determined from the linear regression analysis is displayed. It is these equations that are passed to the online deployment phase. In a field-trial setting, as will be the case within **WP5**, these equations will feature in the secondary substation automation unit (SSAU). The equations are solved in real-time using measurements available at the terminals of a RES unit to determine the reactive power set-point operation of the RES unit from period to period. The round-trip time of a complete cycle from the inverter to the point of calculation and back is important. The quicker the measurement and the required change can be communicated the more accurate and effective the control action.

3.4.2.2 Active Power Loss Minimisation

The objective function for Stage I of the 3-OPF offline simulation is first altered to reflect the objective at hand. In place of equation (3.12), the formulation of equation (3.21) is used in the Stage I analysis that determines the optimal voltage magnitude across all scenarios that **minimises active power losses**. The summation of active power injected at the head of the feeder (represented as a slack generator, g) and power generated from the RES connections less the active power drawn by the customers (represented by ZIP components) will equal the network lost in powering the LV feeder.

$$\min \quad P_{loss}$$

$$P_{loss} = \sum_{s \in Sc} \left(\sum_{g=1}^{G} P_g + \sum_{res=1}^{RES} P_{res} - \sum_{d=1}^{D} P_d \right) \tag{3.21}$$

The sequence of Stages I – IV continues as normal, as per Figure 3.6, apart from Stage III, which is not required to be recalculated. Table 3.3 shows the characteristics of the volt-var curves that would ensure the minimisation of active power losses across all scenarios considered.

Table 3.3 Optimal voltage set-point, slope and intercept of RES systems for Loss Minimisation

RES	*m* [pu]	*c* [pu]	*Vopt* [pu]	Rel. Error [%]
1	-0.0146	0.9839	0.9848	0.09
2	-0.0183	0.9813	0.9835	0.23
3	-0.0105	0.9902	0.9920	0.18
4	-0.0122	0.9874	0.9900	0.27
5	-0.0189	0.9808	0.9819	0.11
6	-0.0046	0.9974	0.9971	-0.03
7	-0.0083	0.9959	0.9955	-0.05
8	-0.0118	0.9938	0.9926	-0.12
9	-0.0117	0.9937	0.9925	-0.12

Similar to the slopes obtained in the minimisation of voltage unbalance (Table 3.2), the slopes presented in Table 3.3 are wholly negative. This is an encouraging indication that correct procedure will be followed in an online deployment phase; such that, the required change in reactive power to bring the measured voltage closer to the target (intercept c) voltage will be positive in the case of under- voltage and negative in the case of over-voltage.

The relative error between the optimal target voltage, V_{opt} (found in Stage I), and the intercept determined from the regression analysis of Stage IV present a stronger case, as compared to the minimisation of voltage unbalance volt-var curves. A maximum error of 0.3% is observed here, indicating that the realistic reactive power capabilities of the RES PV systems can achieve close to optimal voltages across all scenarios considered in the analysis. Figure 3.9 shows the subplots for the RES units displaying the volt-var curve from the linear analysis. In each subplot, the equation determined from the linear regression analysis is displayed.

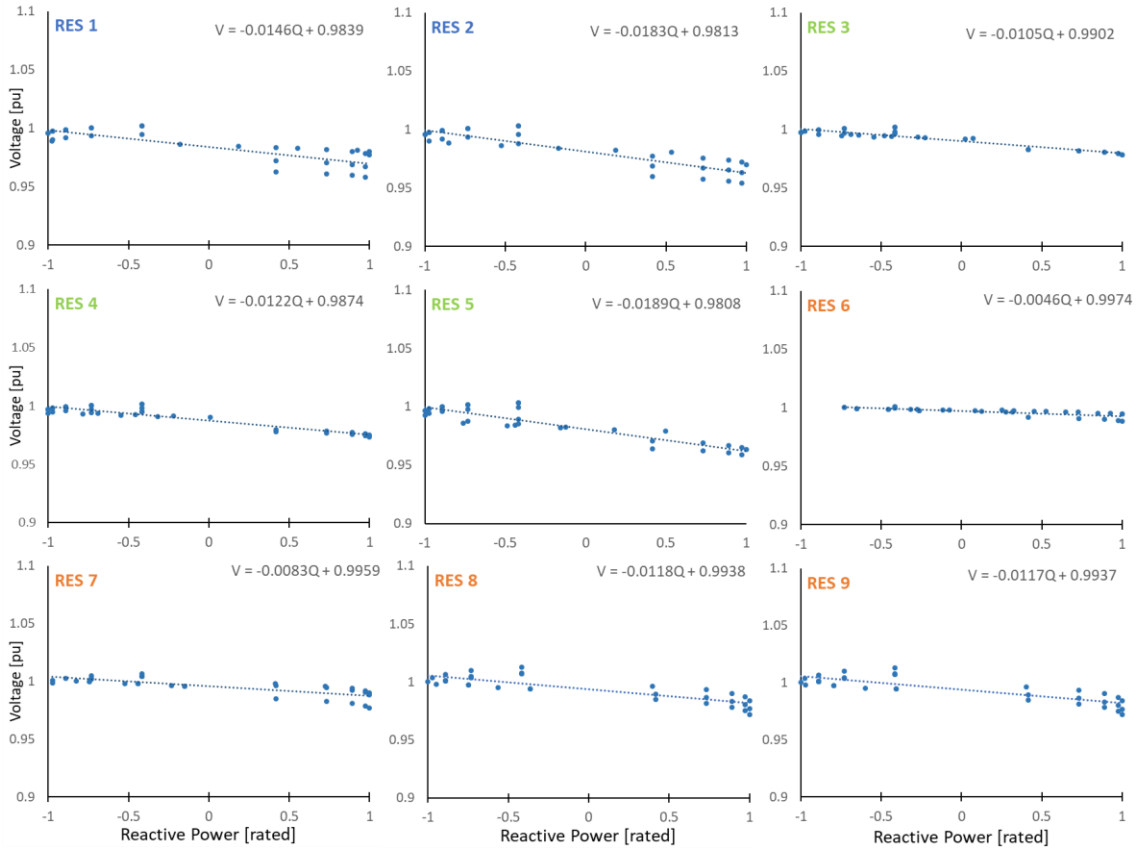

Figure 3.9 Resulting volt-var curves found for the minimisation of active power losses for RES units 1-9, showing optimal voltages and slopes

As is the case for the minimisation of voltage unbalance volt-var curves, the range of voltages observed from fully inductive to fully capacitive never exceed the bounds of rated operation. The maximum range of voltage experienced is that of RES 2, located at the end of the feeder at bus85; a range of 0.051 pu (approx. 11 V) from a maximum of 1.003pu. The RES unit with the minimum range of voltages observed is RES 6, located near the beginning of the feeder; a range of 0.013 pu (approx. 3 V) from a maximum of 1 pu. These voltage values are ascertained using realistic and in-depth consideration of the ZIP composition of demand which gives assurance to their validity in the face of any disparity in demand on LV feeders.

3.4.2.3 Summary of findings

Comparing the volt-var curves obtained in the minimal voltage unbalance case to the loss minimisation case, the relative differences in volt-var curves are a significant finding. Firstly, the incline of the slopes reveal that a RES unit in closer proximity to the transformer at the head of the feeder experiences less of a voltage variation from fully capacitive mode to fully inductive. This is suggestive that the extent of the voltage drop/rise to this point is an easier case to manage when tasked with obtaining the optimal voltage (intercept) of the volt-var curve. In other words, the voltage is *healthier* to begin with due to the reduced impedance path to the source transformer seen by these RES units.

Another point of note is revealed when comparing the slope of the RES units from objective to objective. The slopes are the same for the PV units to two-significant figures, this indicates that the ability of a RES unit to adhere to a voltage or control to a set-point, is more so linked to the topology of the system, the system impedance, and the location of the unit within the system. For this reason, it may be possible to discern a rule-of-thumb for the incline of slopes, based on electrical distance from the transformer.

Comparing the optimal voltages, V_{opt}, for both volt-var sets, reveals that differing objectives of the DSO for these units will result in different behaviour. On a system with high RES penetration or a series of LV feeders like the one of this case study, deploying the AVM technique would result in a significant shift in the operation of the system. This is a strong indication that the desired outcome, to actively manage the voltages while achieving a DSO objective, will operate in a decentralised environment of a field-trial.

Examining the *relative error* columns of Table 3.2 and Table 3.3, verifies that the ability of the RES units to control toward the target voltage. This control is achievable despite the limitation of the reactive power based on the active power output of the unit, as observed in Figure 3.4.

The offline-centralised modelling approach, facilitated by the 3-OPF tool has enabled the identification of an online-decentralised technique for active voltage management for use in real-time operation and control. With the optimal relationships between the voltage magnitude at the terminals of the RES and their reactive power operation now established, Chapter 3.4.3 presents the online deployment of each set of volt-var curves.

3.4.3 Online Deployment - Verification of Volt-var curves

One further series of simulations are conducted to determine the validity of the AVM technique. In a week-long *time-series power flow*, the RES units on the LV feeder are tasked with following their assigned volt-var curves found in the **minimisation of voltage unbalance** case and the **minimisation of active power losses** case. In these simulations, the inverter-based RES units are assigned the volt-var curves of Figure 3.8 and then Figure 3.9.

The operation of these set-points are compared to the operation at **fixed inductive power factor** of 0.95 inductive. This setting constrains the operation of the reactive power output of the units to absorb roughly one-third of the value of active power generated by the PV installations. A fixed lagging power factor is typical for generation sources on distribution systems to reduce the voltage-rise effect from the active power injections.

The bottom-up demand-model is once again utilised to generate a week-long demand profile for the 74 customers modelled on the LV feeder and the 85 customers on the external feeder, modelled in bulk. Historic PV generation data from the UCD campus is used to represent the active power generation from the installations of PV on the LV feeder. **Error! Reference source not found.** subplot (a) illustrates the range of values of active power demand observed at the

head of the feeder. In subplot (b) the rated active power generation from the RES units located on the feeder, for the week-long time-series simulation.

As usual, every time-step considered in the analysis compartmentalises the component of every demand customer into constant impedance, constant current and constant power. The aggregate ZIP exponent of the entire feeder is provided in sub plot (c) of Figure 3.10. This ensures realistic and representative voltage sensitivities are observed on the network as those seen on actual distribution system LV feeders.

Three runs of time-series power flow simulations are conducted utilising the volt-var curves of Figure 3.8 and Figure 3.9 to establish the relationship between the observed voltage measurement at the terminals of the RES units and their set-point operation of reactive power. The results of these simulations are succinctly discussed here.

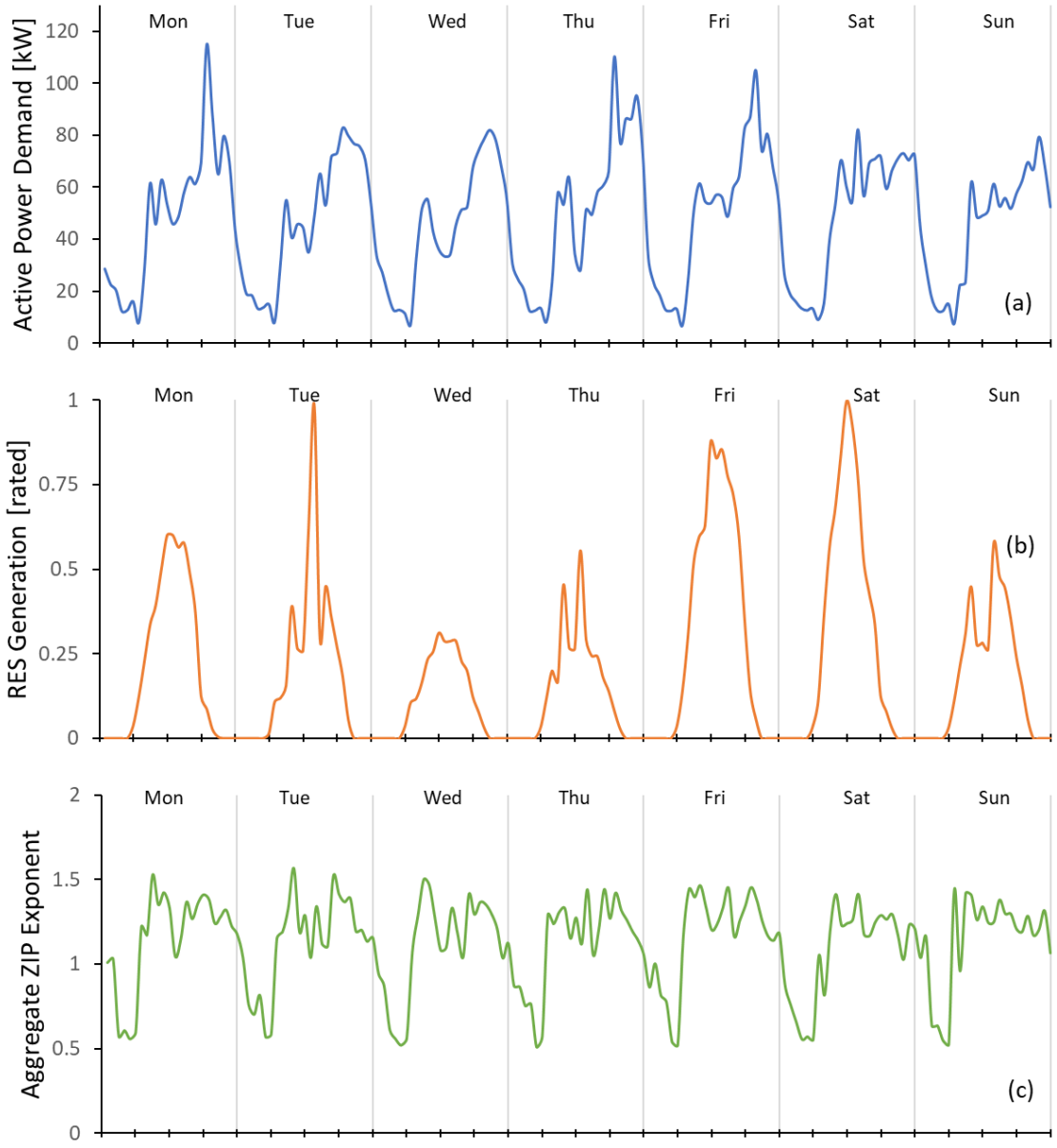

Figure 3.10 Active power demand profile (a), RES rated generation profile (b) and aggregate ZIP exponent of demand (c)

3.4.3.1 Results

Table 3.4 compares the performance metrics of interest to the time-series power flow simulation utilising the volt-var curves found in the offline-analysis. As seen in **Error! Reference source not found.**, the volt-var curves achieve superior results over the course of the week-long time-series simulation, as compared to the fixed inductive power factor base case scenario.

Table 3.4 Comparison of active power loss and voltage metrics

Objective	Active Power Loss [kWh]	Voltage Unbalance	Avg. Voltage [pu]
Min. Power Loss [kW]	**152.74**	0.110	**0.9946**
Min. V. Unbalance	164.31	**0.052**	0.9940
0.95 Ind. Power factor	163.52	0.153	0.9944

A reduction in losses of 6.6% is achieved in the case where the volt-var curves (see Table 3.2) are utilised in the week-long scenario, as compared to fixed power factor operation. An improvement in the voltage unbalance metric, as per equation (3.13), is also observed. Utilising instead the volt-var curves determined for the minimisation of voltage unbalance, achieves a further improved result in these instances, reducing to 0.052 for the entire week. A 66% reduction in voltage unbalance was possible by following the volt-var curves of Figure 3.8.

Figure 3.11 and Figure 3.12 show the set-point operation of reactive power for RES 6 and RES 2 respectively, comparing the use of volt-var curves to minimise voltage unbalance and minimise active power loss. The results of these RES units are highlighted here as they are situated at the beginning end of the feeder, stemming from three-phase supply buses bus02 and bus09 respectively. As seen, the units inject and absorb reactive power within the bounds of their inverter limitations. The range of reactive power values vary across the week-long simulation. There are only a handful of times that the target voltage is achieved at the terminals of the RES without the reactive power support from the RES units. This alone signifies the worth utilising the reactive power capabilities of inverter-based RES units for the purpose of voltage regulation.

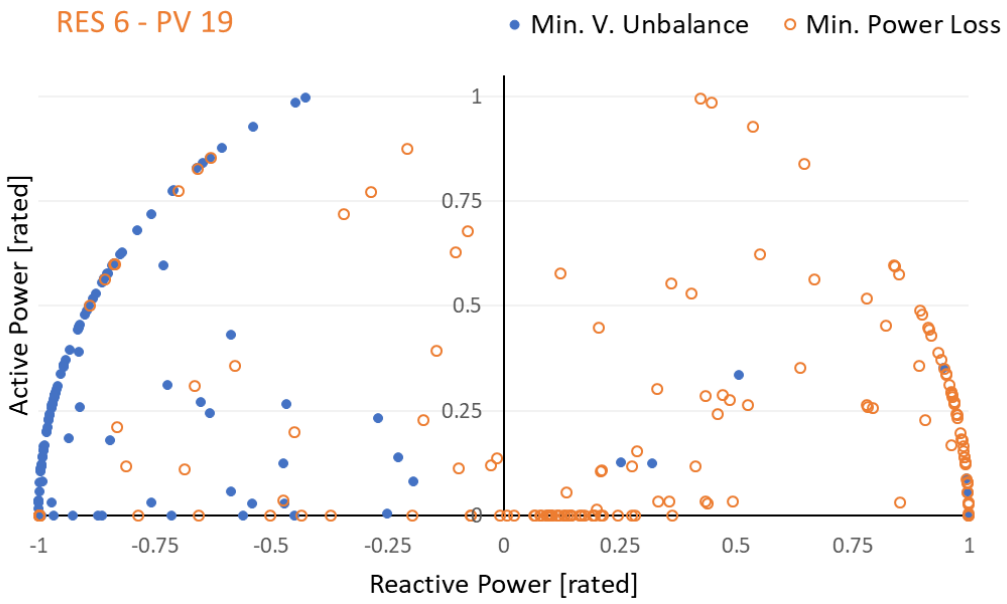

Figure 3.11 Active power and reactive power set-points minimising voltage unbalance and active power loss - RES 6

There are also times where attempting to achieve the target voltage brings the inverter-based RES to its maximum reactive power limit. In these instances, the target voltage is not achieved but rather the RES units are providing the most suitable choice of reactive power as they endeavour to follow the volt-var curves of Figure 3.8 and Figure 3.9. Of note from these results are the contrasting operation of reactive power from objective to objective in the case of RES 6 (Figure 3.11), and the similarities in the operation of reactive power from objective to objective in the case of RES 2 (Figure 3.12).

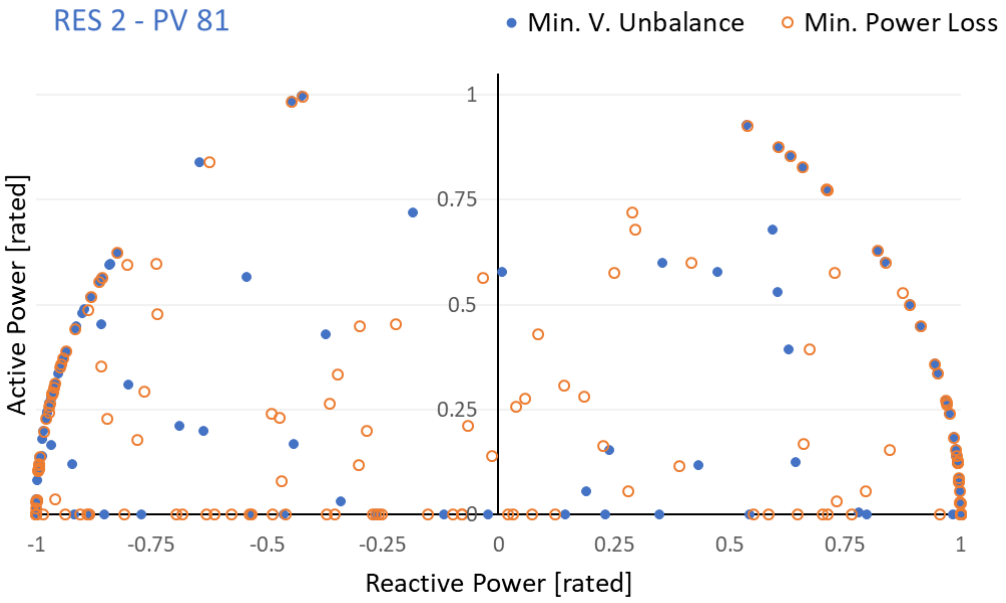

Figure 3.12 Active Power and Reactive Power set-point minimising voltage unbalance and active power loss - RES 2

RES 2 and RES 6 are situated at opposite ends of the feeder and they are connected to different phases. In the case of RES 6, a capacitive operation (leading power factor) is required to adhere to the target voltage that would ensure minimal active power loss, while inductive operation (lagging power factor) is required to reduce the voltage to achieve minimal voltage unbalance between the other phases on the system. In the case that a DSO were to stipulate a change in volt-var curve from one period to the next, this response from the RES unit will undoubtedly invoke an observable reaction to aid and support the objective of the DSO.

In the case of RES 2, there are only minor differences between reactive power operation induced by following the different two volt-var curves. This consistent operation indicates that, for this RES, achieving minimal voltage unbalance will reduce the active power losses on the system. This is not unexpected as RES 2 is situated at the end of the feeder. Differing objective functions, such as the maximisation of energy export, or maximisation of reactive power support to the DSO, may invoke differing behaviours from this unit.

3.5 Conclusions and future work

The AVM technique capitalises on the reactive power capabilities of inverter-based RES units to achieve a desired objective of a distribution system operator on a continual basis. In the offline modelling stage, a four-stage analysis provides the means to determine a dynamic relationship between the voltage at the terminals of a RES and its reactive power operation. These *volt-var curves* enable the decentral operation of RES for voltage management in an online setting, while achieving advantageous performance criteria of the DSO.

The case study of a real LV feeder with 74 customers verifies the AVM technique in a simulation environment, operating within the allowable voltage range and the possible reactive power confinement. Two objectives were investigated and two sets of volt-var curves were formulated

for each RES unit to achieve the **minimisation of voltage unbalance** and, separately, the **minimisation of active power losses**.

The modelling assumptions encapsulated in the offline-modelling stage are key to the success of the AVM technique. POI are identified from pertinent aggregate ZIP exponents to formulate the multi-scenario AC OPF. One optimal voltage target per RES is identified in these diverse conditions that incorporates the entire range of voltage sensitivities experienced on LV feeders.

The deployment of the AVM technique is achievable in a decentral environment. The sole purpose of the reactive power operation is reduced to maintaining the prescribed relationship to the target voltage. In achieving these voltages at the location of RES the optimal operation of the network is guaranteed, making best use of existing assets. Deployment in a field-trial setting is possible by communicating a single measurement at the location of the RES unit, the voltage magnitude. The voltage is used to back calculate the required reactive power response from the RES unit from the equations describing the volt-var curves.

In **WP5** network models will be provided by ESBN on which to run accurate simulations of the differing RES technologies taking part in the field-trials on the Irish trial sites. The AVM technique will be used to determine volt-var curves for these networks. The ICT requirements for deploying the AVM technique are outlined in **D1.3**. In **WP4** the AVM technique will be tested in a testbed with hardware-in-the-loop. In **WP5** the AVM technique will regulate the output of RES in a field-test environment on the Irish distribution system.

4. ICT Monitoring Concepts

This chapter details the system level ICT monitoring concepts with a view toward future tasks in **WP3** and field trial deployment in **WP5.** The requirements on the data handling and a scalability of these techniques are addressed.

4.1 Communication Requirements for Simulations

The **SERVO** platform, allows energy actors (prosumers, aggregators, generators, market participants and system operators defined in **D1.3**) the greatest possible freedom to control generation and load without compromising network existing performance and integrity. The platform is being developed by ESB in Ireland and will be used to implement the voltage control concepts discussed in this deliverable.

4.1.1 Data Access for Simulations

To enable the simulations for both research concepts to occur a time-domain representation of the network data is required. In the context of the Irish grid, where the trials in **WP5** will take place, this data could be provided by extending the SERVO platform with a set of APIs that could in the potentially allow the querying of the historic grid data for use in the simulations. The data gathered will be taken from disparate sources at local level and should be indexed using time and substation for the context of querying at a local level. The data for each substation will be stored in a CIM format which will aim to provide details of the structure of the substation detailing the components involved.

4.1.2 Data Gathering for Simulations

The data will be gathered from components of the network relevant to the trial sites and these components will contain a mix of RES and traditional load and generation sources. The data will be gathered directly from the inverters and will be achieved using a combination of hardware and software components and the technologies used to communicate with each test site will be dependent on the capabilities of the inverters at each component. The software components that will be used will be designed around the protocols that the inverters use to communicate and semantics of the data that each voltage control research concept will require.

The hardware components that may be needed are small electronic devices with integrated software components that will perform the tasks of overcoming potential short comings in the communications technologies that are available at each test site. For the RES the data will be published to an MQTT broker, which is a messaging bus, and will be subscribed to by *SERVO Live* for access to the data which will then be sent to *SERVO Modeller* for CIM formatting and storage. The traditional load and generation sources will be accessed using a combination of SCADA and PMU data which will be accessed also by SERVO Live and sent to SERVO Modeller. Figure 4.1 illustrates a high level conceptual diagram of how the system will operate from the perspective of gathering and accessing the data for the simulations.

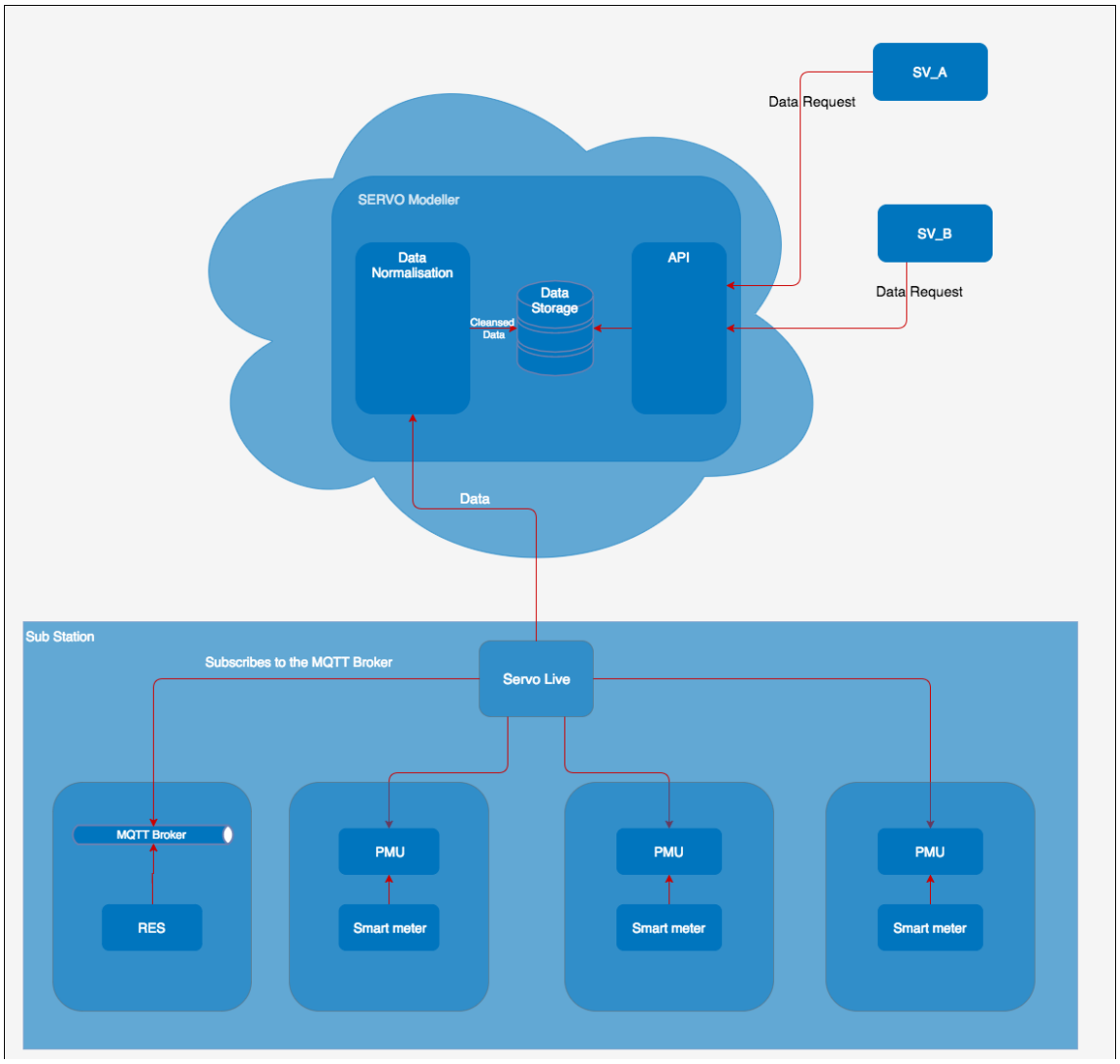

Figure 4.1 SERVO Live and Servo Modeller - a system description

At this stage, the **Dynamic Voltage Stability Monitoring** and the **AVM** techniques can be examined in simulation mode and it is envisaged that **task 3.5** will provide a more realistic examination on the system. This will involve the implementation and deployment of the research concepts and SERVO modeller at substation level. This will allow the implementation of validating the Network Codes at a local level and will ensure that the research concepts have a more real-time representation of the state of the network at a substation level.

4.2 Implementation

The implementation of the DVSM and the AVM techniques in the context of System Level Monitoring from an ICT perspective will involve the deployment of the research concepts at a substation level and communication mechanisms for system monitoring, system control and the application of a sub system to validate the control messages against the network codes using policy based network management techniques. The sections below detail the intended implementation of the above components to enable the effective design of the system that will be deployed in **WP5** on the trial sites.

4.3 Deployment of the Research Concepts

The deployment of the Research Concepts will involve an integration with an existing Sub Station Automation Unit (SSAU) or creation of a dedicated SSAU at a substation level. A deployment of the *SERVO Platform* on the SSAU would perform the functionality of gathering the data, normalising the data and making the data available for the research concepts that

would also be deployed on the SSAU. The SSAU would also perform the task of validating the control messages against the network codes and ultimately sending the control messages to the relevant inverters. The deployment of the research concept algorithms on the SSAU would involve the containerisation of the algorithmic component. This containerisation task will also involve the integration of a suitable communications interface that will allow data connections to be made from the container to the rest of the system for data access and control message execution. The diagram below illustrates the design of the SSAU in the context of performing the system stability studies at a substation level.

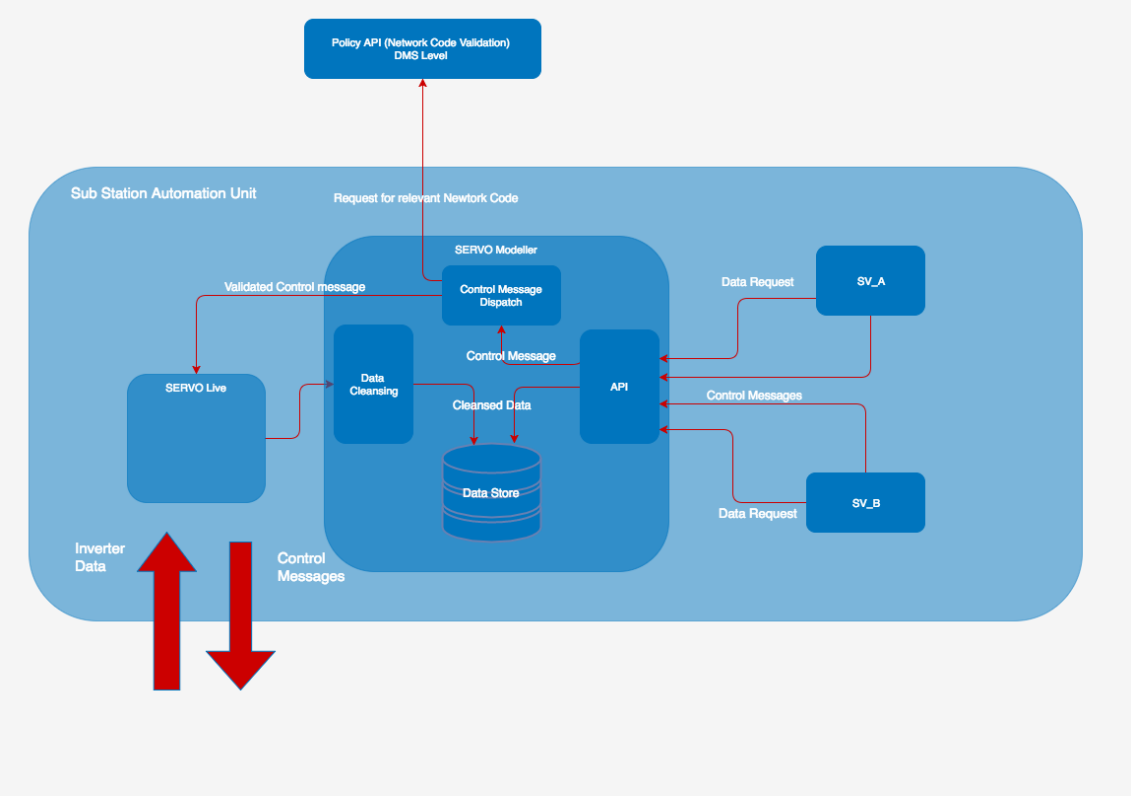

Figure 4.2 Secondary Substation Automation Unit Components

The communication protocols between the components will be a mixture of technologies including REST and MQTT which will be enabled by a communications technology such as 3G, 4G and an integration of the LTE 5G Gateway. These are further explored and defined in **WP4** and the technologies and protocols used will be driven by availability of connectivity, message requirements laid out in **D3.1** and type of experiment being carried out.

4.4 Policy Based Management

Policy based management concepts have their roots in the telecommunications space and provide a standardised model around the management of networks. Their fundamentals are based on the OSI FCAPS model.

FCAPS stands for:

- **Fault Management**: The detection, isolation, alerting and the potential correction of faults occurring within the network.
- **Configuration Management**: The configuration of devices and components on the network.
- **Accounting Management**: The collection of usage levels within the system at all levels of the network it controls.
- **Performance Management**: Ensures that the system is performing at an acceptable and defined level.

- **Security Management**: Ensures that the system devices and components are secure and only accessible by actors authorised to access or control the system.

In the context of a Smart Grid Network these concepts can be applied to the network in software form to all layers of the network and these policies can be informed by a combination of the Network Codes, data transfer format (CIM) validation, security requirements, working limits of the physical components, fault contingency measures and order of precedence of control messages and control devices among others.

All messages and communications that will be sent in the network would be subject to conforming to the network management policies. This approach will enable the deployment of Network Code validation methods and deliver a robust communications solution that can be validated against a mature policy management model. Furthermore, policy based network management can be used to extend the current implementation of networking to investigate the area of autonomics and self-healing. Figure 4.3 details how a typical policy based management system could be implemented in the context of a substation form the perspective of Network Code validation.

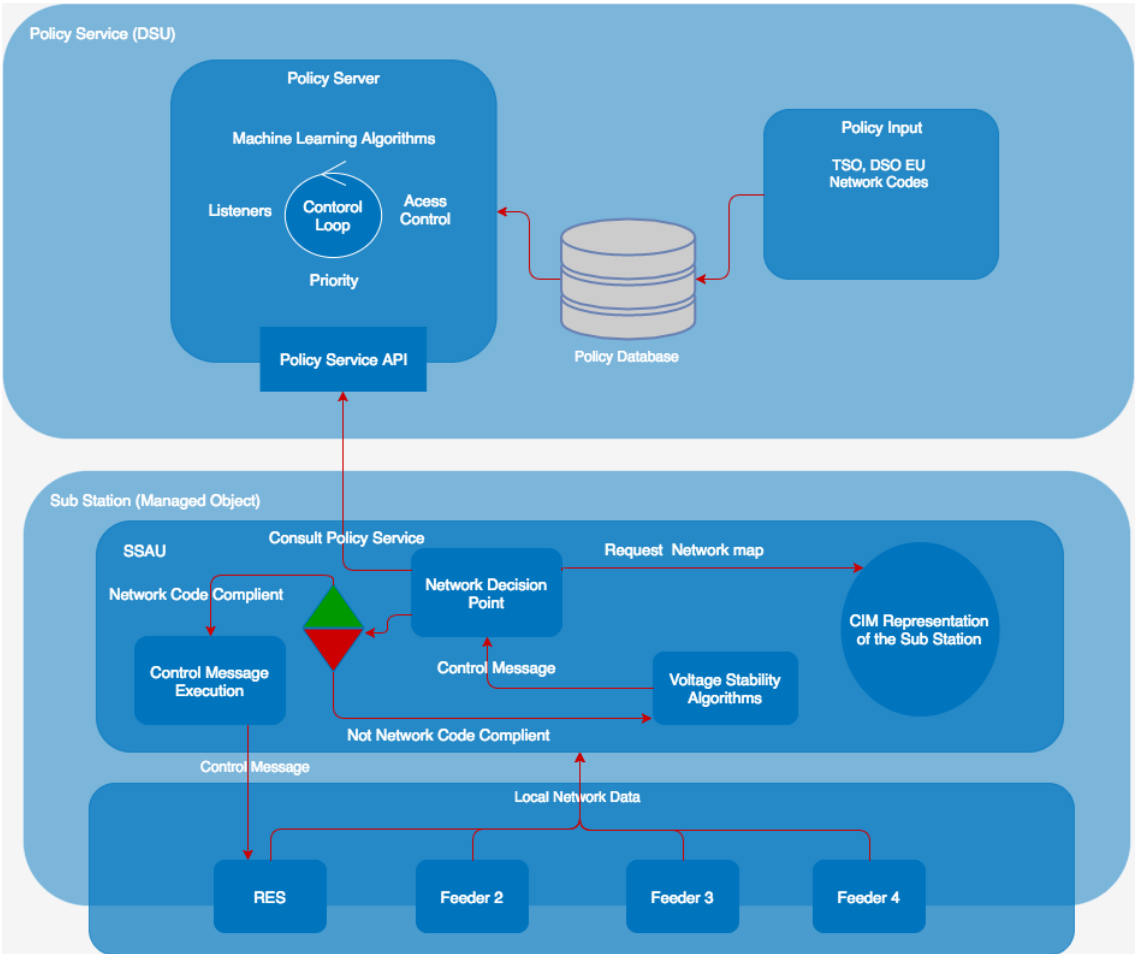

Figure 4.3 Network based policy management implementation

The scenarios below detail potential implementations for network based policy management in the context of the voltage stability research concepts with regards to the Network Codes and order of precedence regarding control devices.

4.4.1 Scenario 1: Voltage Control research concept output causing violation of the Network Codes

This scenario pertains to a control message generated by the SV_A research concept and passed by a controller to the inverters influencing the MVAr output that may not provide enough dynamic voltage control capacity as stated in the Network Code reference OC4.4.1.2. If the

application of policy based management was to be implemented, the network codes would be codified in software and deployed to the relevant controllers and the by policy. Based on the network codes, the controller would then make an informed choice on whether to execute the control message or not. Figure 4.4 shows a schematic logic diagram describing a network code violation comparing a non-policy based management to a scenario with policy based management enforcing a network code.

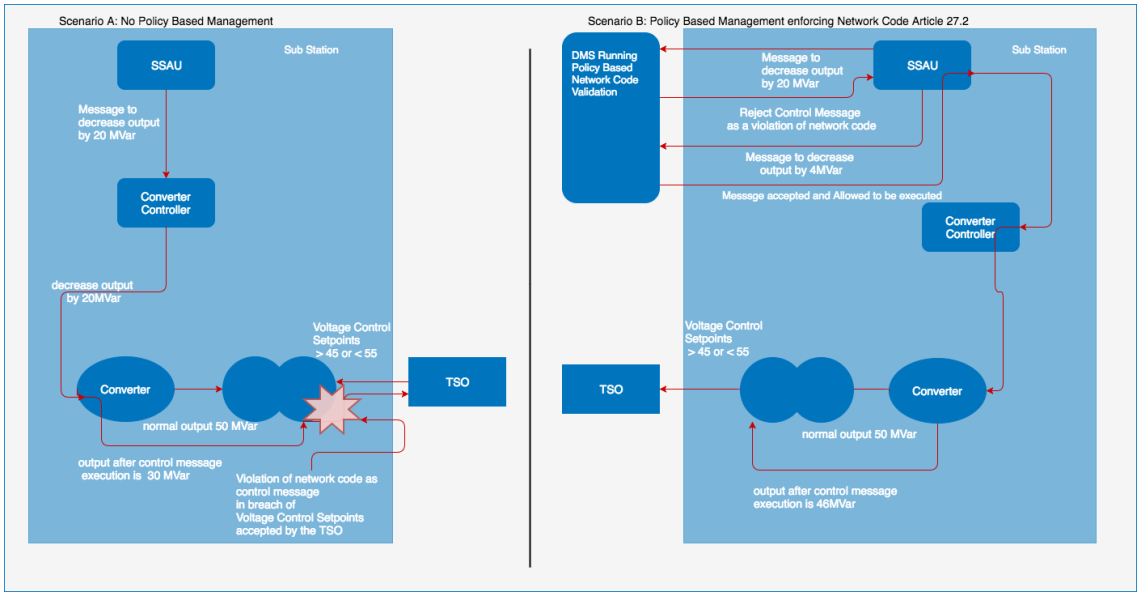

Figure 4.4 Network code violation policy management implementation

4.4.2 Scenario 2: Data Concurrency and Message Collision

This scenario explains the potential implications of control message collision and how they can be avoided using the implementation of policy based network management. The flow chart below, in Figure 4.5, represents a simple network scenario with two controllers having control over the same device. Controller A is the dominant one, for this context it could be at a Substation Control level, and Controller B, for this context it could be at a field level. Both controllers can execute messages and the context of the messages generated by both involve a computation based on readings and a message based on that computation is sent to the device to affect the readings being generated.

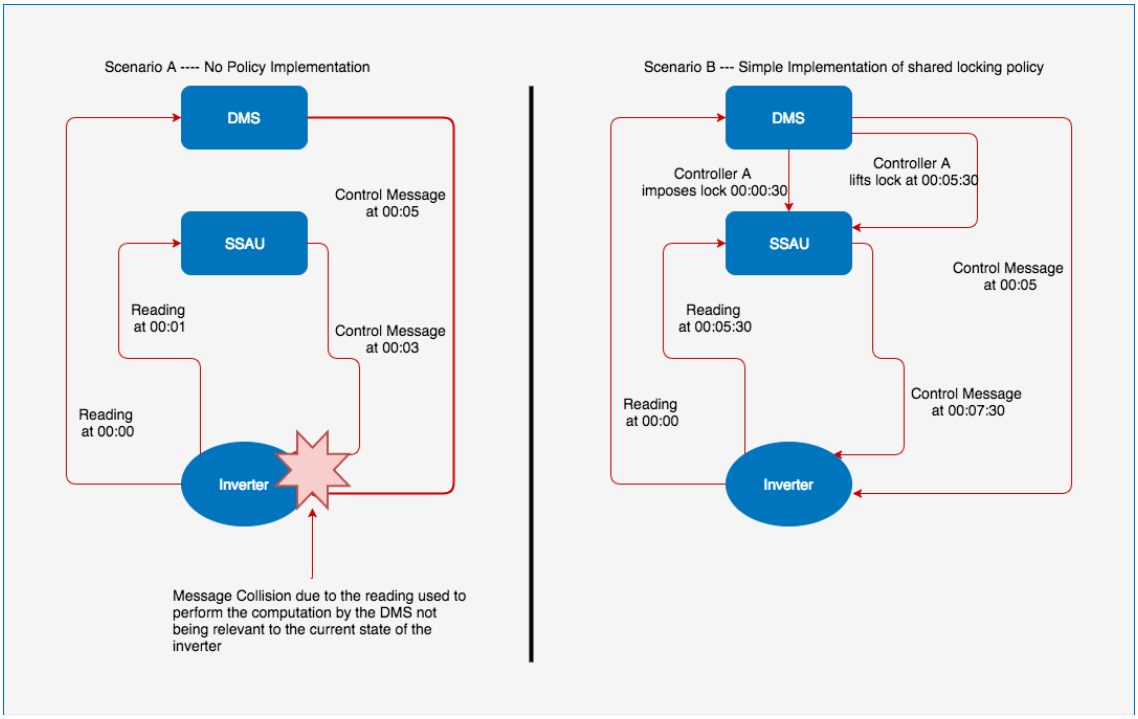

Figure 4.5 Policy based collision control example

4.5 Software Implementation of Network Codes

From investigating the status of the Network Codes from an Irish perspective it appears that there is a disconnect and no real aggregation from the Network Codes detailed by the DSO, TSO and by the ones specified by the EU. While there are definite similarities in the high-level headings, there is no linkage from the point of view basic naming conventions which is a large factor from not only a standardisation perspective but also poses a critical barrier when it comes to codifying the Network Codes for implementation. To achieve a codification of the Network Codes it is key to consider all actors, as in the TSO, DSO and the EU, when developing the standard by which they are used and aggregated. One such approach would be to combine each network code under a common code heading that will encompass each actor defined network code, with each actor defined network code holding the most relevance at the level of the system that is most relevant to that actor. This will also hold the caveat of using the network code developed by the EU as a conflict resolution mechanism where a conflict occurs between the TSO and DSO instances of a specific Network Code. The example below contains a textual representation of the same code taken from the EU commission guidelines, the [ESB Networks Distribution Code (DSO)] (https://www.esbnetworks.ie/who-we-are/distribution-code) and the EirGrid Grid Code (TSO) and codified to create a common code that will encompass all three representations. Currently there are no suitable codes defined in the context of RES at the LV level of the grid and there is the potential that a local RES installation would fall short in capacity required to comply with the network codes in their current form. The implementation and codification of the network codes will form a standard process and when new codes are developed they can be implemented in the same way as the existing ones.

A demonstration of the codification of the network codes is provided in annex A.3. This demonstration is based on the EU Commission guidelines on voltage control and reactive power management.

5. Conclusion

Task 3.2 and the results provided here in **D3.2** act as a proof-of-concept of the proposed voltage control and stability concepts.

The DVSM technique of SV_A is a decentralized approach towards distribution grids with high penetration of RES. The two main components of the SV_A algorithm are the stability monitoring concept and the virtual output impedance control methodology. The solution to the former is addressed is this deliverable and the solution to the latter will be the content of future deliverable **D3.5**. Task 3.2 consolidates the validation of the proposed extension of voltage stability concepts based on Middlebrook theory to distribution networks.

The GNC method is adopted for the case of an exemplary LV distribution grid. A 3-node LV feeder was considered both in grid connected mode and islanded mode. Stability analysis and time domain simulations were performed to see the impact of controller gains and the PLL gains. Coherency between the time domain simulations and the characteristic loci obtained from GNC based stability analysis in the frequency domain establishes proof of concept. In the future deliverable **D3.3,** the presence of active rectifiers interfacing DC loads will be considered, which will represent futuristic loads realistically.

The deployment of the AVM technique of SV_B is achievable in a decentral environment. The sole purpose of the reactive power operation from RES is reduced to maintaining the prescribed relationship to the target voltage. In achieving these voltages at the location of RES the optimal operation of the network is guaranteed, making best use of existing assets. Deployment in a field-trial setting is possible by communicating a single measurement at the location of the RES unit: the voltage magnitude. The voltage is used to back calculate the required reactive power response from the RES unit from the equations describing the volt-var curves.

The investment required to deploy alternate omniscient centralised voltage control solutions and prove the approach by way of a field-trial is unrealistic. A preferable alternative is the AVM technique, a modular and decentralised approach that connects RES on a case-by-case basis. Until such a time that every node voltage on distribution systems are communicated or can be estimated within satisfactory tolerance, a decentralised approach must be taken. The AVM decentralised technique underpins the fundamental prerequisites for deploying a central approach, as such, further investment would in future see the technique amalgamate into a central approach.

This research effort has been a critical step in validating the voltage control concepts. Developing the technology and demonstrating the hardware functioning in a live environment will raise the TRL of both voltage concepts. For the concepts to become a reality, ICT development is to be undertaken in future tasks within **WP3**, building on content already delivered in **D1.2** and **D1.3**. Within **WP5** The Dynamic Voltage Stability Monitoring and AVM technique and are to be deployed in a field-trial operated by the Irish DSO, ESBN. Within **WP4** the techniques are to be demonstrated on a test-platform. The SERVO platform is to facilitate the deployment of the techniques in the field-trials, whereby suitable infrastructure is to be installed, further to that presented in **D5.1**. Ancillary service provision and recommendation for network codes will take form with the interaction of the technology on a live-network.

6. References

[1] R. D. Middlebrook, “Input filter considerations in design and application of switching regulators,” pp. 366–382, 1976.

[2] A. Riccobono and E. Santi, “Comprehensive Review of Stability Criteria for DC Power Distribution Systems,” *IEEE Trans. Ind. Appl.*, vol. 50, no. 5, pp. 3525–2535, 2014.

[3] M. Stojic and D. Siljak, “Generalization of Hurwitz, Nyquist and Mikhailov stability criteria,” vol. 10, no. 3, pp. 250–254, 1965.

[4] A. G. J. MacFarlane and I. Postlethwaite, “The generalized Nyquist stability criterion and multivariable root loci,” vol. 25, pp. 81–127, 1977.

[5] D. Siljak, “A note on the generalized Nyquist criterion,” vol. 11, no. 2, p. 317, 1966.

[6] B. Wen, D. Boroyevich, R. Burgos, P. Mattaveli, and Z. Shen, “Inverse Nyquist Stability Criterion for Grid-Tied Inverters,” vol. 32, no. 2, pp. 1548–1556, 2017.

[7] J. Kimball and M. Zawodniok, “Reducing Common-Mode Voltage in Three-Phase Sine-Triangle PWM With Interleaved Carriers,” *IEEE Trans. Power Electron.*, vol. 26, no. 8, pp. 2229–2236, 2011.

[8] B. Mirafzal, M. Saghaleini, and A. . Kaviani, “An SVPWM-Based Switching Pattern for Stand-Alone and Grid-Connected Three-Phase Single-Stage Boost Inverters,” *IEEE Trans. Power Electron.*, vol. 26, no. 4, pp. 1102–1111, 2011.

[9] B. Wen, D. Boroyevich, R. Burgos, P. Mattaveli, and Z. Shen, “Analysis of D-Q Small-Signal Impedance of Grid-Tied Inverters,” *IEEE Trans. Power Electron.*, vol. 31, no. 1, pp. 675–687, 2016.

[10] A. Riccobono, E. Liegmann, A. Monti, C. Dezza, and E. E. Santi, “‘Online wideband identification of three-phase AC power grid impedances using an existing grid-tied power electronic inverter,’” in *2016 IEEE 17th Workshop on Control and Modeling for Power Electronics*, 2016.

[11] A. Barkley and E. Santi, “Online Monitoring of Network Impedances Using Digital Network Analyzer Techniques,” in *Applied Power Electronics Conference and Exposition, 2009. APEC 2009. Twenty-Fourth Annual IEEE, Washington, DC*, 2009.

[12] D. Martin, E. Santi, and A. Barkley, “‘Wide bandwidth system identification of AC system impedances by applying pertubations to an existing converter,’” in *Energy Conversion Congress and Exposition (ECCE), 2011 IEEE*, 2011.

[13] B. Miao, R. Zane, and D. Maksimovic, “System Identification of Power Converters With Digital Control Through Cross-Correlation Methods,” *IEEE Trans.Power Electron*, vol. 20, no. 5, pp. 1093–1099, 2005.

[14] T. Roinila, T. Messo, and A. Aapro, “Impedance measurement of three phase systems in DQ-domain: Applying MIMO-identification techniques,” in *2016 IEEE Energy Conversion Congress and Exposition (ECCE), Milwaukee, WI*, 2016.

[15] A. Emadi, A. Khaligh, C. H. Rivetta, and G. A. Williamson, “Constant power loads and negative impedance instability in automotive systems: Definition modeling stability and control of power electronic converters and motor drives,” *IEEE Trans. Veh. Technol.*, vol. 55, no. 4, pp. 1112–1125, 2006.

[16] L. Herrera, W. Zhang, and J. Wang, “Stability Analysis and Controller Design of DC Microgrids With Constant Power Loads,” *IEEE Trans. Smart Grid*, vol. 8, no. 2, pp. 881–888, 2017.

[17] A. O’Connell and A. Keane, “Volt-var curves for photovoltaic inverters in distribution systems,” *IET Gener. Transm. Distrib.*, vol. 11, no. 3, pp. 730–739, 2017.

[18] K. McKenna and A. Keane, “Open and Closed-Loop Residential Load Models for Assessment of Conservation Voltage Reduction,” *IEEE Trans. Power Syst.*, vol. PP, no. 99, 2016.

[19] P. Richardson, D. Flynn, and A. Keane, “Local Versus Centralized Charging Strategies for Electric Vehicles in Low Voltage Distribution Systems,” *Smart Grid, IEEE Transactions on*, vol. 3, no. 2. pp. 1020–1028, 2012.

[20] A. O’Connell and A. Keane, “Multi-period three-phase unbalanced optimal power flow,” in *Innovative Smart Grid Technologies Conference Europe (ISGT-Europe), 2014 IEEE PES*, 2014, pp. 1–6.

[21] A. O’Connell, “Unbalanced distribution system voltage optimisation,” in *PES Innovative Smart Grid Technologies Conference Europe (ISGT-Europe), 2016 IEEE*, 2016, pp. 1–6.

[22] A. O’Connell, D. Flynn, and A. Keane, “Rolling Multi-Period Optimization to Control Electric Vehicle Charging in Distribution Networks,” *IEEE Trans. Power Syst.*, vol. 29, no. 1, pp. 340–348, Jan. 2014.

[23] K. McKenna and A. Keane, “Residential Load Modeling of Price-Based Demand Response for Network Impact Studies,” *IEEE Trans. Smart Grid*, vol. 7, no. 5, pp. 2285–2294, Sep. 2016.

[24] M. Bakhtvar and A. Keane, “A study of operation strategy of small scale heat storage devices in residential distribution feeders,” in *PES Innovative Smart Grid Technologies Conference Europe (ISGT-Europe), 2017 IEEE*, 2017, pp. 1–6.

7. List of Abbreviations

B2B Business to Business
BMS Building management system
CAPEX CAPital EXpenditure
CENELEC European Committee for Electro technical Standardization
CEP Complex Event Processing
COTS Commercial off-the-shelf
CPMS Charge Point Management System
CSA Cloud Security Alliance
EMS Decentralised energy management system
DER Distributed Energy Resources
DMS Distribution Management System
DMTF Distributed Management Taskforce
DSE Domain Specific Enabler
EAC Exploitation Activities Coordinator
ERP Enterprise Resource Planning
ESB Electricity Supply Board
ESCO Energy Service Companies
ESO European Standardisation Organisations
ETP European Technology Platform
ETSI European Telecommunications Standards Institute
GE Generic Enabler
GNC Generalised Nyquist Criterion
HEMS Home Energy Management System
HiL Hardware in the Loop
HV High Voltage
I2ND Interfaces to the Network and Devices
ICT Information and Communication Technology
IEC International Electro-technical Commission
IoT Internet of Things
KPI Key Performance Indicator
LV Low Voltage
M2M Machine to Machine
MPLS Multiprotocol Label Switching
MV Medium Voltage
NIST National Institute of Standards and Technology
O&M Operations and maintenance
OPEX OPerational Expenditure
OPF Optimal Power Flow
PCC Point of Common Coupling
PLL Phase Lock Loop
PM Project Manager
PMT Project Management Team
POI Points of Interest
PPP Public Private Partnership
PWM Pulse Width Modulation
PMU Phasor Measurement Unit
QEG Quality Evaluation Group
S3C Service Capacity; Capability; Connectivity
SCADA Supervisory Control and Data Acquisition
SDH Synchronous Digital Hierarchy
SDN Software Defined Networks
SDOs Standards Development Organisations
SET Strategic Energy Technology
SET Strategic Energy Technology
SG-CG Smart Grid Coordination Group
SGSG Smart Grid Stakeholders Group

SME	Small & Medium Enterprise
SoA	State of the Art
SON	Self Organizing Network
SRF	Synchronous Reference Frame
SS	Secondary Substation
SSAU	Secondary Substation Automation Unit
TL	Task Leader
TM	Technical Manager
TRL	Technology Readiness Level
VPP	Virtual Power Plant
WP	Work Package
WPL	Work Package Leader

8. List of Figures

Figure 1.1 Relations between Deliverables in WP3 and other work packages 7
Figure 2.1 Inverter with current control structure 9
Figure 2.2 Closed loop model of three-phase grid-connected inverter 9
Figure 2.3 Simulation scenarios 11
Figure 2.4 Stability analysis results 11
Figure 2.5 Comparison of Id step response (Id = 200A to 300A) 12
Figure 2.6 Comparison of I_q step response (I_d = 200A to 300A) 12
Figure 2.7 PLL model 13
Figure 2.8 Impact of PLL 14
Figure 2.9 3-node LV feeder: Grid connected case 15
Figure 2.10 3-node LV feeder: Microgrid case 15
Figure 2.11 Grid connected mode: Stable case: Characteristic loci at PCC1 and PCC3 16
Figure 2.12 Grid connected case: Stable case: Inverter currents and voltages 16
Figure 2.13 Grid connected mode: Unstable case: Inverter currents and voltages 16
Figure 2.14 Grid connected mode: Unstable case: Characteristic loci at PCC1 and PCC2 17
Figure 2.15 Islanded mode: Stable case: Inverter currents and voltages 17
Figure 2.16 Islanded mode: Unstable case: Inverter currents and voltages 18
Figure 2.17 Frequency response comparison for stable and unstable PLL configurations 18
Figure 3.1 Active power demand of 74 customers supplied to LV feeder identifying POI 21
Figure 3.2 Aggregate ZIP composition of 74 customers identifying POI 22
Figure 3.3 Workflow of the 3-OPF modelling tool 23
Figure 3.4 P-Q capability chart of a generic PV system 25
Figure 3.5 Sample volt-var curve showing orientation and bounds of voltage and reactive power 26
Figure 3.6 Procedure to determine objective governed volt-var curve using the 3-OPF modelling tool 27
Figure 3.7 Network topology showing customer point of connection, phase and RES location 28
Figure 3.8 Resulting volt-var curves found for the minimisation of voltage unbalance for RES units 1-9, showing optimal voltages and slopes 30
Figure 3.9 Resulting volt-var curves found for the minimisation of active power losses for RES units 1-9, showing optimal voltages and slopes 31
Figure 3.10 Active power demand profile (a), RES rated generation profile (b) and aggregate ZIP exponent of demand (c) 33
Figure 3.11 Active power and reactive power set-points minimising voltage unbalance and active power loss - RES 6 34
Figure 3.12 Active Power and Reactive Power set-point minimising voltage unbalance and active power loss - RES 2 35
Figure 4.1 SERVO Live and Servo Modeller - a system description 38
Figure 4.2 Secondary Substation Automation Unit Components 39
Figure 4.3 Network based policy management implementation 40

Figure 4.4 Network code violation policy management implementation 41
Figure 4.5 Policy based collision control example 42
Figure A.1.1 Equivalent impedance diagram: Grid connected case……52
Figure A.1.2 Equivalent impedance diagram: Microgrid case 53

9. List of Tables

Table 3.1 Location, phase, three-phase supply node and capacity of RES connections 28
Table 3.2 Optimal voltage set-point, slope and intercept of RES systems for minimal voltage unbalance 29
Table 3.3 Optimal voltage set-point, slope and intercept of RES systems for Loss Minimisation 31
Table 3.4 Comparison of active power loss and voltage metrics 34
Table A.1.1 Rating of the Inverter 50
Table A.1.2 LCL filter parameter 50
Table A.1.3 Control parmeter 50
Table A.1.4 Grid impedance parameters 50
Table A.2.1 Description of sets, parameters and variables used within 3-OPF 54
Table A.2.2 Series resistance (R), reactance (X) and shunt conductance (G) and susceptance (B) by cable type from node and phase i to node and phase j 55
Table A.3.1 Voltage ranges at the connection point between 110 kV and 300 kV 56
Table A.3.2 Voltage ranges at the connection point between 300 kV and 400 kV 56
Table A.3.3 Operating Voltage Range 57
Table A.3.4 Maximum voltage at the connection point with generators 57

Annex

A.1 Additional elements of the DVSM

A.1.1 Grid Connected Case System parameters

Table A.1.1 Rating of the Inverter

Parameter	Rating
DC link voltage (Vdc)	700 V
Switching frequency (fsw)	40 kHz
Filter inductance (Lt)	0.5 mH
Inductive coil internal resistance (Rt)	0.1 Ω
Filter capacitance (Co)	10 μF
Grid voltage (phase - phase) (Vg)	400 V
Grid frequency (f_0)	50 Hz
Local resistive load (RL)	30 Ω

In the case of current controlled (CC) inverters, an LCL filter is used. The parameters of the LCL filter is given by Table A.1.2.

Table A.1.2 LCL filter parameter

Parameter	Rating
Filter inductance (Lt)	2 mH
Grid side inductance (Lg)	0.5 mH
Inductive coil internal resistance (Rt)	0.1 Ω
Filter capacitance (Co)	20 μF
Local resistive load (RL)	30 Ω

Table A.1.3 Control parmeter

Current Control Parameter	Values
K_{cp}	6.47×10^{-3}
K_{ci}	50.24

Table A.1.4 Grid impedance parameters

Impedance branch	Parameter	Values
Z_{g1}	R_{g1}	0.25 Ω
	L_{g1}	1 mH
	C_{g1}	15 μH
Z_{g2}	R_{g2}	0.25 Ω

Z_{g3}	L_{g2}	5 mH
	R_{g3}	0.25 Ω
	L_{g3}	1 mH

A.1.2 Grid impedance modelling

A generic RL impedance branch in *dq* frame is modelled as follows:

$$Z_{RL}(s) = \begin{bmatrix} sL + R & -\omega L \\ \omega L & sL + R \end{bmatrix} \quad \text{A.1}$$

Where s is the complex frequency variable or Laplace variable ($s = j\omega$). Similarly, the impedance model of a generic capacitive branch in dq is as follows:

$$Z_C(s) = \begin{bmatrix} sC & -\omega C \\ \omega C & sC \end{bmatrix} \quad \text{A.2}$$

The impedance of Z_{g1} is a parallel combination of RL branch and C branch. Z_{g2} and Z_{g3} are same as the RL branch impedance.

Grid impedance during Case 1:

$$Z_G = \left[Z_{g1}^{-1} + Z_{g2}^{-1} \right]^{-1} \quad \text{A.3}$$

Grid impedance during Case 2:

$$Z_G = \left[Z_{g1}^{-1} + Z_{g3}^{-1} \right]^{-1} \quad \text{A.4}$$

A.1.3 Inverter impedance modelling

A 3-phase inverter with an LC filter is considered. L_t is the inductance with coil resistance R_t, C_o is the output filter capacitance and R_L is the local resistive load of the inverter. The inductor current is denoted as i_{Ld} and i_{Lq} and the capacitor voltage is denoted by v_{cd} and v_{cq}. The grid current is denoted by i_{gd} and i_{gq}. Let V_{DC} be the DC side voltage which is assumed to be stiff. Additionally, the PLL dynamics are neglected.

Let the state variables x be defined by the inductor current and capacitor voltages.

$$x = \begin{bmatrix} i_{Ld} & i_{Lq} & v_{cd} & v_{cq} \end{bmatrix} \quad \text{A.5}$$

By Kirchhoff's voltage and current law, we have the following dynamic equations.

$$L_t \frac{di_{Ld}}{dt} = \frac{d_d v_{DC}}{2} + \omega L_t i_{Lq} - i_{Ld} R_t - v_{cd} \quad \text{A.6}$$

$$L_t \frac{di_{Lc}}{dt} = \frac{d_q v_{DC}}{2} - \omega L_t i_{Ld} - i_{Lq} R_t - v_{cq} \quad \text{A.7}$$

$$C_o \frac{dv_{cd}}{dt} = i_{Ld} + \omega C_o v_{cq} - \frac{v_{cd}}{R_L} - i_{gd} \quad \text{A.8}$$

$$C_o \frac{dv_{cq}}{dt} = i_{Lq} - \omega C_o v_{cd} - \frac{v_{cq}}{R_L} - i_{gq} \quad \text{A.9}$$

By linearising the above equations with d as the input and i_L as the output, we get the control transfer function G_{id}. Similarly, by linearising with i_g as the input and v_c as the output, we get the open loop admittance transfer function Y_{ol}. The closed loop admittance Y_{cl} is obtained using the following expression:

$$Y_{cl} = \left[I + G_{id}(G_{ci} - G_{dec})\right]^{-1} Y_{ol} \quad \text{A.10}$$

The controller transfer function is G_{ci} and the decoupling transfer function is given by G_{dec}. By considering the impact of PLL, the following expression gives the output admittance of the inverter:

$$Y_{cl,pll} = [I + G_{id}\,(G_{ci} - G_{dec})]^{-1}\left[Y_{ol} + G_{id}\left\{-(G_{ci} - G_{dec})G_{i,pll} + G_{d,pll}\right\}\right] \quad \text{A.11}$$

A.1.4 3-node LV feeder parameter

Each of the cable impedances are assumed to be equal and known. The inductance of the cable between every node is 10 μH and the resistance of the cable between every node is 0.5Ω. An example of the equivalent grid impedance diagram evaluated at PCC3 for the grid connected case and islanded case is shown in Figure A.1.1 and Figure A.1.2 respectively.

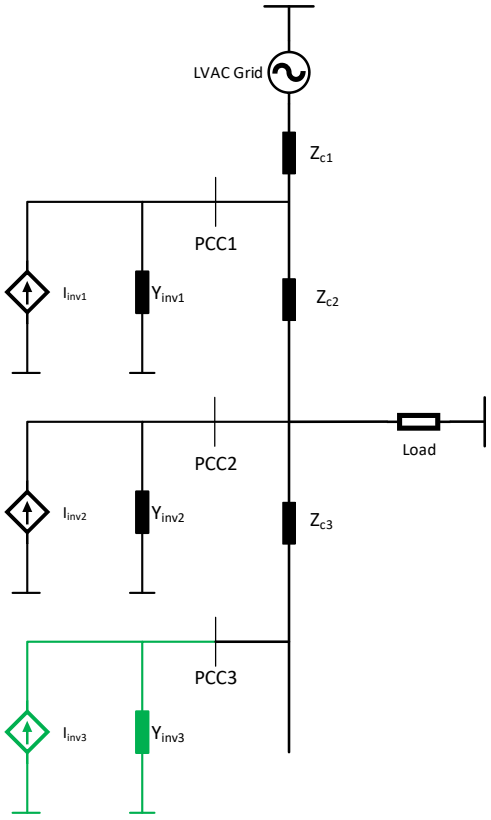

Figure A.1.1 Equivalent impedance diagram: Grid connected case

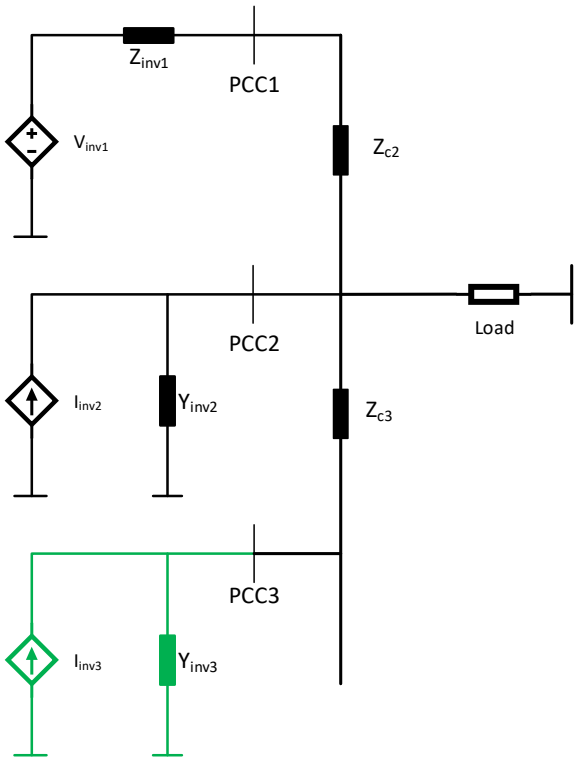

Figure A.1.2 Equivalent impedance diagram: Microgrid case

The equivalent admittance of the inverter is Y_{inv3} and the grid impedance is given by the Thevenin equivalent of the complex circuit represented in black as seen from the node PCC3.

A.2 Additional elements of the AVM technique

This annex lists the various elements of the AVM technique not provided in the summary text of Chapter 3.

Quantities within an optimisation problem are defined as either *parameters* that take on a fixed value or *variables* that are free to change. An offline four-stage study is conducted using an ACOPF approach, as detailed in Chapter 3.3.1. A description of the parameters and variables used in the 3-OPF tool are provided in Table A.2.1.

Table A.2.1 Description of sets, parameters and variables used within 3-OPF

B	Set of buses
L	Set of branches
G	Set of generators
D	Set of demands
RES	Set of RES units
Φ	Set of phases
Sc	Set of scenarios
m	Slope
c	Intercept
$V_{b,\varphi}$	Voltage (at bus $b \in B$ and $\varphi \in \Phi$)
V^+, V^-	Upper and lower voltage limit
$Vopt_{b,\varphi}$	Optimal RES target voltage (at bus $b \in B$ and $\varphi \in \Phi$)
$Vunb_{b,\varphi}$	Voltage unbalance (at bus $b \in B$ and $\varphi \in \Phi$)
$\overline{V}_b^{abc}$	Average voltage magnitude (at bus $b \in B$)
$I_{l,\varphi}$	Current (through branch $l \in L$ and $\varphi \in \Phi$)
$I_{l,\varphi}^+$	Current limit (of branch $l \in L$ and $\varphi \in \Phi$)
P_d, Q_d	Active and reactive power (of demand $d \in D$)
P_d^+, P_d^-	Maximum and minimum active power limit (of demand $d \in D$)
Q_d^+, Q_d^-	Maximum and minimum reactive power limit (of demand $d \in D$)
P_g, Q_g	Active and reactive power (of generator $g \in G$)
P_g^+, P_g^-	Maximum and minimum active power limit (of generator $g \in G$)
Q_g^+, Q_g^-	Maximum and minimum reactive power limit (of generator $g \in G$)
P_{res}, Q_{res}	Active and reactive power (of RES $res \in RES$)
P_{res}^+, P_{res}^-	Maximum and minimum active power limit (of RES $res \in RES$)
Q_{res}^+, Q_{res}^-	Maximum and minimum reactive power limit (of RES $res \in RES$)
Z_P	Constant impedance component for active power demand

I_P	Constant current component for active power demand
P_P	Constant power component for active power demand
Z_Q	Constant impedance component for reactive power demand
I_Q	Constant current component for reactive power demand
P_Q	Constant power component for reactive power demand

In Table A.2.2 the electrical properties of the cables used in the case studies of Chapter 3 are provided on an ohm per kilometre basis.

Table A.2.2 Series resistance (R), reactance (X) and shunt conductance (G) and susceptance (B) by cable type from node and phase i to node and phase j

Cable	i	j	**R** ohm/km	**X** ohm/km	**G** ohm/km	**B** ohm/km
LV 4-core NAKBA 4x70	a	a	0.727	0.259	1.676	-0.313
LV 4-core NAKBA 4x70	a	b	0.275	0.219	-0.543	-0.041
LV 4-core NAKBA 4x70	a	c	0.284	0.183	-0.516	0.065
LV 4-core NAKBA 4x70	b	a	0.275	0.219	-0.543	-0.041
LV 4-core NAKBA 4x70	b	b	0.711	0.288	1.676	-0.313
LV 4-core NAKBA 4x70	b	c	0.275	0.219	-0.543	-0.041
LV 4-core NAKBA 4x70	c	a	0.284	0.183	-0.516	0.065
LV 4-core NAKBA 4x70	c	b	0.275	0.219	-0.543	-0.041
LV 4-core NAKBA 4x70	c	c	0.727	0.259	1.676	-0.313
LV AYCY 1x25/16	a	a	1.548	0.527	0.396	-0.489
LV AYCY 1x25/16	a	b	0.000	0.000	0.000	0.000
LV AYCY 1x25/16	a	c	0.000	0.000	0.000	0.000
LV AYCY 1x25/16	b	a	0.000	0.000	0.000	0.000
LV AYCY 1x25/16	b	b	1.548	0.527	0.396	-0.489
LV AYCY 1x25/16	b	c	0.000	0.000	0.000	0.000
LV AYCY 1x25/16	c	a	0.000	0.000	0.000	0.000
LV AYCY 1x25/16	c	b	0.000	0.000	0.000	0.000
LV AYCY 1x25/16	c	c	1.548	0.527	0.396	-0.489

A.3 Codified Network Codes

This annex chapter details codified examples of network codes stipulating voltage limits. These are presented to demonstrate this activity of the SSAU and SERVO in field trials taking place in **WP5**.

Article 27.1 In accordance with Article 18, each TSO shall endeavour to ensure that during the normal state the voltage remains in steady-state at the connection points of the transmission system within the ranges specified in Table A.3.1 and Table A.3.2.

Table A.3.1 Voltage ranges at the connection point between 110 kV and 300 kV

Synchronous Area	Voltage Range [pu]
Continental Europe	0.90 – 1.118
Nordic	0.90 – 1.118
Great Britain	0.90 – 1.10
Ireland and Northern Ireland	0.90 – 1.118
Baltic	0.90 – 1.118

Table A.3.2 Voltage ranges at the connection point between 300 kV and 400 kV

Synchronous Area	Voltage Range [pu]
Continental Europe	0.90 – 1.05
Nordic	0.90 – 1.05
Great Britain	0.90 – 1.05
Ireland and Northern Ireland	0.90 – 1.05
Baltic	0.90 – 1.097

CC8.3.2 During Transmission System disturbances or following transmission faults:

(a) 400kV system: 350kV to 420kV;

(b) 220kV system: 200kV to 245kV;

(c) 110kV system: 99kV to 123kV.

Some Transmission System disturbances (e.g. earth faults, lightning strikes) will result in short-term Voltage deviations outside the above ranges.

DPC4.2.2 The DSO shall operate the Distribution System so as ensure that the voltage at the supply terminals, as defined in EN 50160, complies with that standard. The Low Voltage range tolerance shall be 230V +/- 10%. The resulting voltage at different points on the system depends on several factors, but at the Connection Point with Customers can be expected to be in accordance with Table A.3.3 under steady state and normal operating conditions.

Table A.3.3 Operating Voltage Range

Nominal Voltage [kV]	Highest Voltage [kV]	Lowest Voltage [kV]
0.23	0.253	0.207
0.4	0.44	0.360
10	11.1	Variable according to operating conditions. Information on particular location on request by the user concerned
20	22.1	
38	43	
110	120	

Higher maximum voltages can arise at the Connection Point with Generators as per Table A.3.4, specified by clause **DCC10.5**.

Table A.3.4 Maximum voltage at the connection point with generators

Nominal Voltage [kV]	Highest Voltage [kV]
0.23	0.253
0.4	0.44
10	11.3
20	22.5
38	43.8
110	120

A codified representation of the Network Code around reactive power and voltage control is provided below. The codified version should not contain the full text of the code. The text of the code will need to be distilled into a quantified into a temporal, numeric or categorical value so as its implementation can be simplified when used in a live scenario.

```
{
        ....
                vc.rpm.1 :{
                eu: a27.1,
                tso: CC8.3.2,
                dso: DPC4.2.2
        }
        ....
}
```

For example, each rule would be parsed and normalised, where possible, to have a quantifiable value, a27.1 would become:

```
eu: {
        "110-300" : {
            "min" : 0.90pu,
            "max" : 1.118pu
        },
```

```
        "300-400" : {
            "min" : 0.90pu,
            "max" : 1.05pu
        }
}
```

CC8.3.2 would become:

```
tso : {
        400 : {
            "min" : 370,
            "max" : 410
        },
        220 : {
            "min" : 200,
            "max" : 245
        },
        110 : {
            "min" : 99,
            "max" : 123
        }
}
```

and DPC4.2.2 (d) would become:

```
dso : {
        400 : {
            "min" : 360,
            "max" : 440
        },
        230 : {
            "min" : 207,
            "max" : 253
        },
        110 : {
            "max" : 120
        },
        38 : {
            "max" : 43
        },
        20 : {
            "max" : 22.1
        },
        10 : {
            "max" : 11.1
        }
}
```

The complete representation of the rule surrounding Reactive Power Management thresholds that must be applied to Voltage control would when codified would look like this:

```
vc.rp.1 :{
   eu: {
        "110-300" : {
            "min" : 0.90pu,
            "max" : 1.118pu
        },
        "300-400" : {
```

```
            "min" : 0.90pu,
            "max" : 1.05pu
        }
    },
    tso : {
        400 : {
            "min" : 370,
            "max" : 410
        },
        220 : {
            "min" : 200,
            "max" : 245
        },
        110 : {
            "min" : 99,
            "max" : 123
        }
    },
    dso : {
        400 : {
            "min" : 360,
            "max" : 440
        },
        230 : {
            "min" : 207,
            "max" : 253
        },
        110 : {
            "max" : 120
        },
        38 : {
            "max" : 43
        },
        20 : {
            "max" : 22.1
        },
        10 : {
            "max" : 11.1
        }
    }
}
```

A normalised codified schema of network codes would allow a reading or a control message to be compared to control the system by policy; the policy in this case would mean that, no control message generated would, when its consequences are measured, be allowed to violate the network code vc.rpm.1.

To explore this from the perspective of a 110 kV system and a control message that would cause the voltage level in the context of reactive power to drop to 80 kV. From the DSO perspective, this is not in violation as there is no minimum specified in the DSO version of the Network Codes but it is a violation of the TSO version of the Network Codes as it has a minimum voltage level of 99 kV. In this case, where there is conflict between both DSO and TSO versions of the Network Codes the EU Commission's version would be consulted and in this case when calculated based on 0.90 pu the minimum voltage allowed is 99 kV.